AD-A135 854 PERFORMANCE ANALYSIS OF DECENTERED UNSTABLE RESONATORS (U) AIR FORCE INST OF TECH WRIGHT-PATTERSON AFB OH SCHOOL OF ENGINEERING S M RINALDI DEC 82 1/2

UNCLASSIFIED AFIT/GEO/PH/82D-12 F/G 9/1 NL

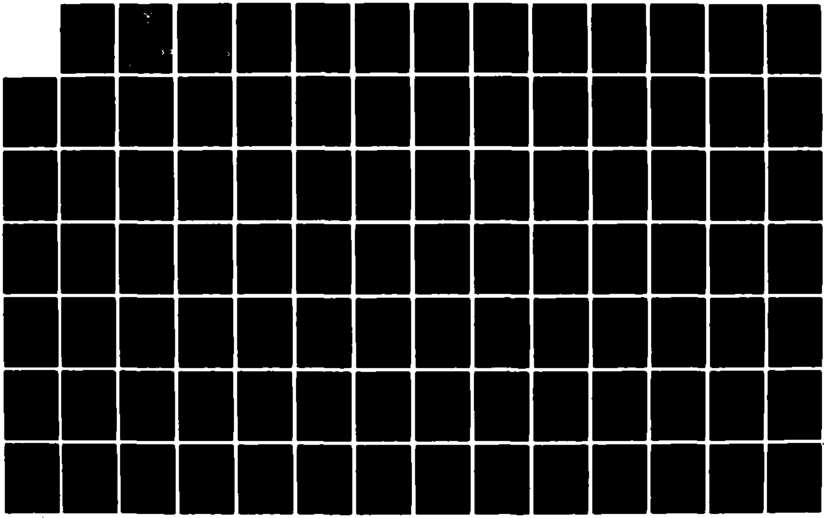

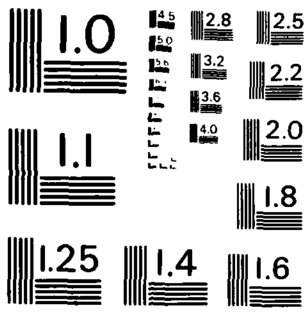
1.0
4.5
5.0
2.8
2.5
3.2
2.2
3.6
4.0
2.0
1.1
1.8
1.25
1.4
1.6

1

AD-A135 954

DEPARTMENT OF THE AIR FORCE
AIR UNIVERSITY (ATC)

AIR FORCE INSTITUTE OF TECHNOLOGY

Wright-Patterson Air Force Base, Ohio

AFIT/GEO/PH/82D-12

PERFORMANCE ANALYSIS OF DECENTERED UNSTABLE RESONATORS

THESIS

AFIT/GEO/PH/82D-12

Steven M. Rinaldi
2Lt USAF

AFIT/GEO/PH/82D-12

PERFORMANCE ANALYSIS OF DECENTERED UNSTABLE RESONATORS

THESIS

Presented to the Faculty of the School of Engineering
of the Air Force Institute of Technology
Air University
in Partial Fulfillment of the
Requirements for the Degree of
Master of Science in Electrical Engineering

by

Steven M. Rinaldi, B.S.E.E.

2Lt USAF

Graduate Electro-Optics

December 1982

Preface

The purpose of this study was to examine the mode eigenvalues, far field beam quality, and far field beam steering of decentered, unstable resonators. Because of the complex nature of mode modeling, much of the anlaysis performed was numerical instead of theoretical. It is hoped that the lack of explicit formulae and mathematical developments will not detract from the value of the numerical analyses.

As with any major undertaking, this study would not have been possible without the support, aid, and encouragement of many people. Much gratitude and appreciation is due Lt Col John Erkkila, my advisor, for his constant guidance and understanding, especially during the final phases of this project. My thanks are due Capt Mark Rogers for the many useful discussions of resonators and his help with the computer (a monster by any measure!). Sharon Gabriel, my typist, deserves much appreciation for her excellent work. And finally, my sincerest appreciation goes to my family and friends for their support and words of encouragement throughout this endeavor.

Steven M. Rinaldi

Table of Contents

Table of Contents (Cont'd)

List of Figures

List of Figures (Cont'd)

List of Tables

Abstract

The mode eigenvalues, far field integrated intensity, and far field beam steering angles of unstable, decentered strip resonators were studied. The resonators examined had magnifications of 2.0 and equivalent Fresnel numbers in the range $9.3 \leq N_{eq} \leq 9.9$. The resonator modes were calculated by the asymptotic method of Horwitz.

Two equivalent Fresnel numbers for the decentered resonators were defined. The fundamental and second-order mode eigenvalues exhibited periodicities in the equivalent Fresnel numbers. The mode separation was observed to be a function of the amount of decenter and the two equivalent Fresnel numbers. The cusps of the first two eigenvalues were cyclic in N_{eq}.

The far field integrated intensity was computed for spot sizes of one, two, and three Airy disks. The percentage of total power deposited in a given spot size increased as the decenter increased. Beam quality instabilities were observed in all modes.

The beam steering angles of the first four modes were calculated. The angles fluctuated about the optic axis as the decenter was increased. The fundamental mode had significantly lower beam steering than the higher-order modes.

PERFORMANCE ANALYSIS OF

DECENTERED UNSTABLE RESONATORS

I. Introduction

Background

Optical cavities may be categorized in two general classes: the stable and the unstable resonators. Stable resonators are characterized by well-defined mod[illegible] The mode volumes of such cavities are generally quit[illegible] [illegible]all. Output coupling of the modes is usually accomplis[illegible]d by transmission through a mirror or other optical element. Consequently, the output power levels achievable in stable resonator designs are limited to relatively low values. Unstable resonators are characterized by large mode volumes. The modes are outcoupled via diffraction around one or both of the resonator mirrors. The output power levels of unstable resonator lasers are not limited to low values; hence, unstable resonators are used in high power applications.

The modes in a stable resonator are well-defined and easily calculated. The modes are generally described in terms of the Hermite-Gaussian or Laguerre-Gaussian functions (Ref 1:1324). The modes of unstable resonators are not so simply described. They must be computed by

using one of several different numerical techniques. One solution technique of particular interest is the asymptotic method (Ref 2), which was used to determine the modes in this study.

The geometry of a general resonator is depicted in Figure 1-1. M is the geometric magnification, a_1 and a_2 are the linear half-widths of mirrors M_1 and M_2, respectively, R_1 and R_2 are the radii of curvature of the mirrors, and L is the axial length of the resonator. The well-known g parameters are given by

$$g_i = 1 - \frac{R_i}{L} \qquad i = 1,2 \tag{1.1}$$

If $0 \leq g_1 g_2 \leq 1$, the resonator is stable. Otherwise, the resonator is classified as unstable.

The equivalent Fresnel number is defined by

$$N_{eq} = \frac{1}{2}\left(M - \frac{1}{M}\right) \frac{a_2^2}{2\lambda' L g_1} \tag{1.2}$$

λ' is the radiation wavelength. This parameter is related to the number of Fresnel zones intercepted by mirror M_2.

The geometry of misaligned and decentered resonators is depicted in Figure 1-2. It can easily be shown (Ref 3: 19-23) that a misalignment of mirror M_2 is equivalent to a decenter of that mirror:

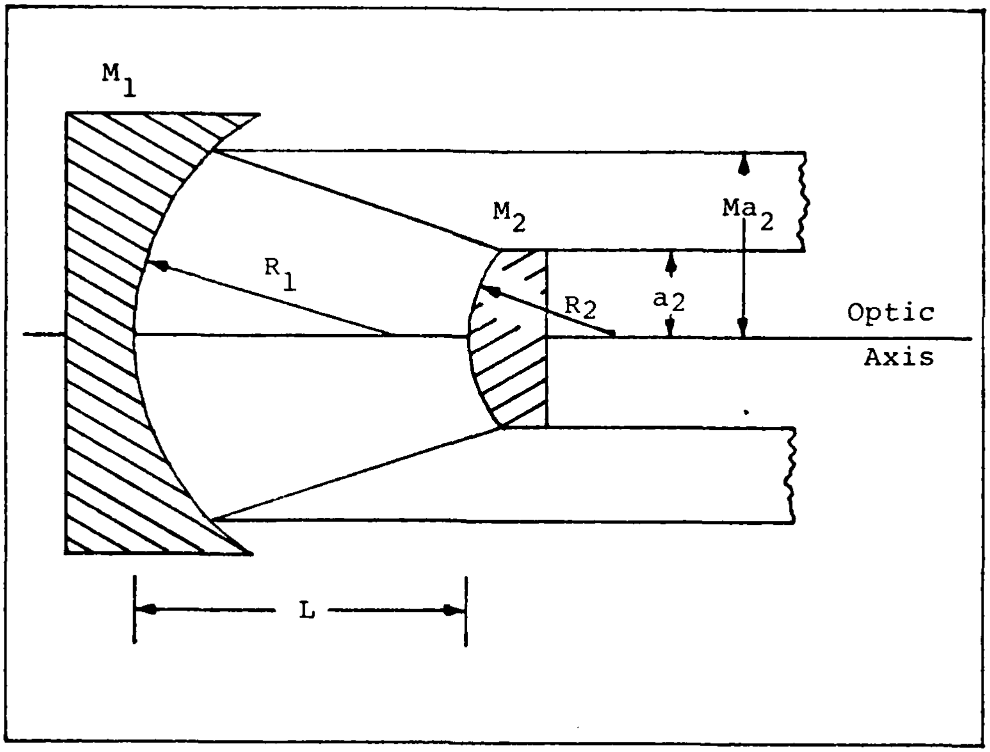

Figure 1-1. Geometry of an Unstable Laser Resonator

$$\delta = \frac{a_2}{\lambda} \frac{\theta}{N_{eq}} \frac{M+1}{M-1} \qquad (1.3)$$

where δ is the fractional offset of M_2 and θ is the angle through which M_2 is tilted. As a result, off-axis resonators can be analyzed as misaligned resonators, and vice-versa.

The confocal resonator is a special type of cavity. The g parameters of this resonator must satisfy the relationship:

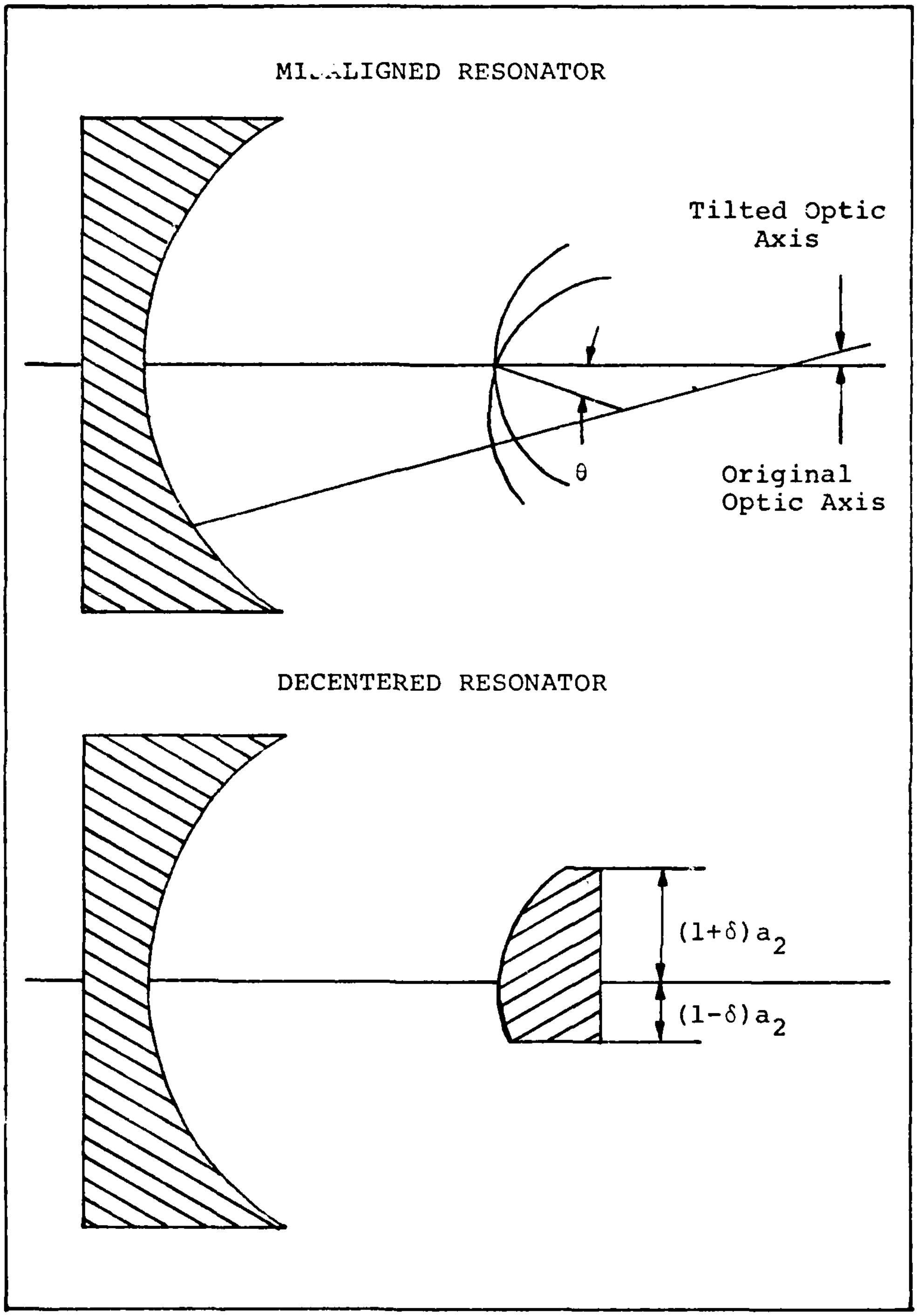

Figure 1-2. Geometries of Misaligned and Decentered Resonators

$$g_1 + g_2 = 2g_1g_2 \tag{1.4}$$

The output beam of a confocal resonator is collimated. In the geometric optics limit, the beam is a plane wave. This is a limiting value of the spherical wave mode (in the geometric optics limit) of a general unstable resonator.

The Asymptotic Method

This section discusses the asymptotic method of solving for bare, strip resonator modes. As this solution technique is derived in detail elsewhere (Refs 2, 3, 4, 5), the following development is simply a brief outline.

The generalized integral equation describing the resonator modes is

$$\lambda u(x) = \int_a^b K(x,y)u(y)\,dy \tag{1.5}$$

where $u(x)$ is the mode, λ is the mode eigenvalue, and $K(x,y)$ is the kernel of the integral. For a decentered resonator, Eq (1.5) becomes

$$\lambda g(x) = \sqrt{\frac{it}{\pi}} \int_{-1+\delta}^{1+\delta} g(y)\ \exp[-it(y-x/M)^2]\,dy \tag{1.6}$$

where

$$g(x) = e^{i\pi N_{eq} x^2} u(x) \tag{1.7}$$

$$t = \pi MF = \frac{\pi M a_2}{2\lambda' L g_1} \tag{1.8}$$

In Eq (1.6), the half-width a_2 of mirror M_2 has been normalized to unity. The integration is thus taken over the surface of M_2, with the decenter accounted for. y is a dummy variable of integration.

$g(x)$ can be approximated as a unit amplitude spherical wave plus a finite series of higher-order edge-diffracted waves. This expansion is given by

$$g(x) = 1 + \sum_{n=1}^{N} [a_n F_n(x) + b_n G_n(x)] \tag{1.9}$$

where

$$F_n(x) = -\sqrt{\frac{M_{n-1}}{4i\pi t}} \; \frac{\exp[-it(1-x/M^n)^2/M_{n-1}]}{(1 - x/M^n)} \tag{1.10}$$

$$G_n(x) = -\sqrt{\frac{M_{n-1}}{4i\pi t}} \; \frac{\exp[-it(1+x/M^n)^2/M_{n-1}]}{(1 + x/M^n)} \tag{1.11}$$

$$M_n = \sum_{k=0}^{n} M^{-2k}$$

Equations (1.9), (1.10), and (1.11) are substituted into Eq (1.6). The resultant integral equation is evaluated by the method of stationary phase. The final result is

$$\lambda\{1 + \sum_{n=1}^{N}[a_n F_n(x) + b_n G_n(x)]\} = 1 + F_1(x) + G_1(x)$$

$$+ \sum_{n=1}^{N}[a_n F_{n+1}(x) + b_n G_{n+1}(x)]$$

$$+ F_1(x) \sum_{n=1}^{N} [a_n F_n(\beta) + b_n G_n(\beta)]$$

$$+ G_1(x) \sum_{n=1}^{N} [a_n F_n(\alpha) + b_n G_n(\alpha)] \qquad (1.13)$$

where

$$\alpha = -1 + \delta \qquad (1.14)$$

$$\beta = 1 + \delta \qquad (1.15)$$

As shown in Chapter II, Eq (1.13) can be reduced to a polynomial expression in λ with known coefficients. The equation can be solved numerically for the eigenvalues. The coefficients a_n and b_n are then easily computed. Finally, the mode $u(x)$ is calculated from Eqs (1.9) and (1.7).

Objectives

The objectives of this study are to examine the behavior of the eigenvalues and the far field modes as functions of the decenter parameter δ . Specifically, the objectives are:

(1) To determine how the eigenvalues evolve as δ is increased from zero. The relationships between the cusping nature of the first two eigenvalues and the equivalent Fresnel numbers $N_{eq,L}$ and $N_{eq,U}$ will be explored (see Chapter II).

(2) To determine how the far field integrated intensity changes as a function of δ for the first four modes.

(3) To explore the relationship between the far field beam steering angles and δ for the first four modes.

(4) To develop a simple set of design criteria for unstable resonators based on the observations listed above.

Assumptions and Limitations

The assumptions and limitations of Reference 3 apply to this study, as the computer model developed in that work was used to predict the resonator modes. The following additional assumptions and limitations are made:

(1) The Fraunhofer approximation is sufficient to calculate the far field mode patterns. This approximation is valid if the far field patterns are calculated at distances far from the resonator output aperture. Since this separation was taken to be infinite, this approximation is valid.

(2) The computer code used to predict the resonator modes is valid for decenters of $0.0 \le \delta \le 0.9$. Weiner asserts that this is essentially true (Ref 6:1831), based on comparisons of modes calculated by the asymptotic method and the power method (Ref 7).

(3) Only bare strip resonators with magnification $M = 2$ and equivalent Fresnel numbers in the range $9.3 \le N_{eq} \le 9.9$ will be studied. The results of Appendix A, however, are valid for general M and N_{eq} values.

Throughout this study, reference will be made to the "geometric mode." This is the geometric mode of a confocal resonator - a uniform plane wave. Upon emergence from the resonator, the mode will have a uniform "annular" profile.

Organization

In Chapter II, a general theory of mode eigenvalues is presented. The eigenvalue polynomial equation is developed, and theoretical predictions about eigenvalues of

decentered resonators are made. The far field integrated intensity and beam steering are discussed in Chapter III, based on a Fourier optics treatment of the geometric mode. In Chapter IV, the major sources of numerical error that exist in the computer code that determines the far field modes, integrated intensity, and beam steering are evaluated. The study results are presented in Chapter V. The general unstable resonator design criteria are presented in Chapter VI, and the overall conclusions and recommendations are relegated to Chapter VII.

II. Theory of Mode Eigenvalues

A general theory of the mode eigenvalues is presented. The polynomial equation used to compute the eigenvalues in the asymptotic approximation is derived for completeness, even though its development exists elsewhere (Refs 3:28-30; 4:24-29). The concept of two equivalent Fresnel numbers for decentered resonators is developed, and its relationship to the mode eigenvalues is discussed.

Background Theory of Eigenvalues - Aligned Resonators

The general form of the integral equation describing the round trip propagation through a resonator is

$$\lambda u(x) = \int_a^b K(x,y)u(y)dy \tag{2.1}$$

This is an eigenvalue problem. λ is the eigenvalue and the integration is the operator.

After a round trip through the resonator under steady state conditions, the mode must be essentially unchanged in form. After the propagation, the mode $u'(x)$ must be given by

$$u'(x) = \lambda u(x) \tag{2.2}$$

At every point on the wavefront, the amplitude is scaled

by the magnitude of the eigenvalue and the phase is shifted by the phase of the eigenvalue.

The fraction of energy coupled out of the resonator is related to the eigenvalue. For strip resonators,

$$(\text{Outcoupled Energy Fraction})_i = 1 - \frac{|\lambda_i|}{M} \tag{2.3}$$

where i refers to the i^{th} mode and M is the geometric magnification of the resonator.

The symmetric mode eigenvalues exhibit a periodicity when plotted against the equivalent Fresnel number of the resonator. Notably, the separation between the magnitudes of the first and second symmetric mode eigenvalues has maxima at approximately

$$N_{eq} = n + \frac{3}{8} \quad , \quad n=0,1,2,\ldots \tag{2.4}$$

and minima at approximately

$$N_{eq} = n + \frac{7}{8} \quad , \quad n=0,1,2,\ldots \tag{2.5}$$

This behavior is apparent in Figure 2-1. This plot displays the magnitudes of the first seven (symmetric and anti-symmetric) mode eigenvalues. A periodic nature of the eigenvalues is rather clear.

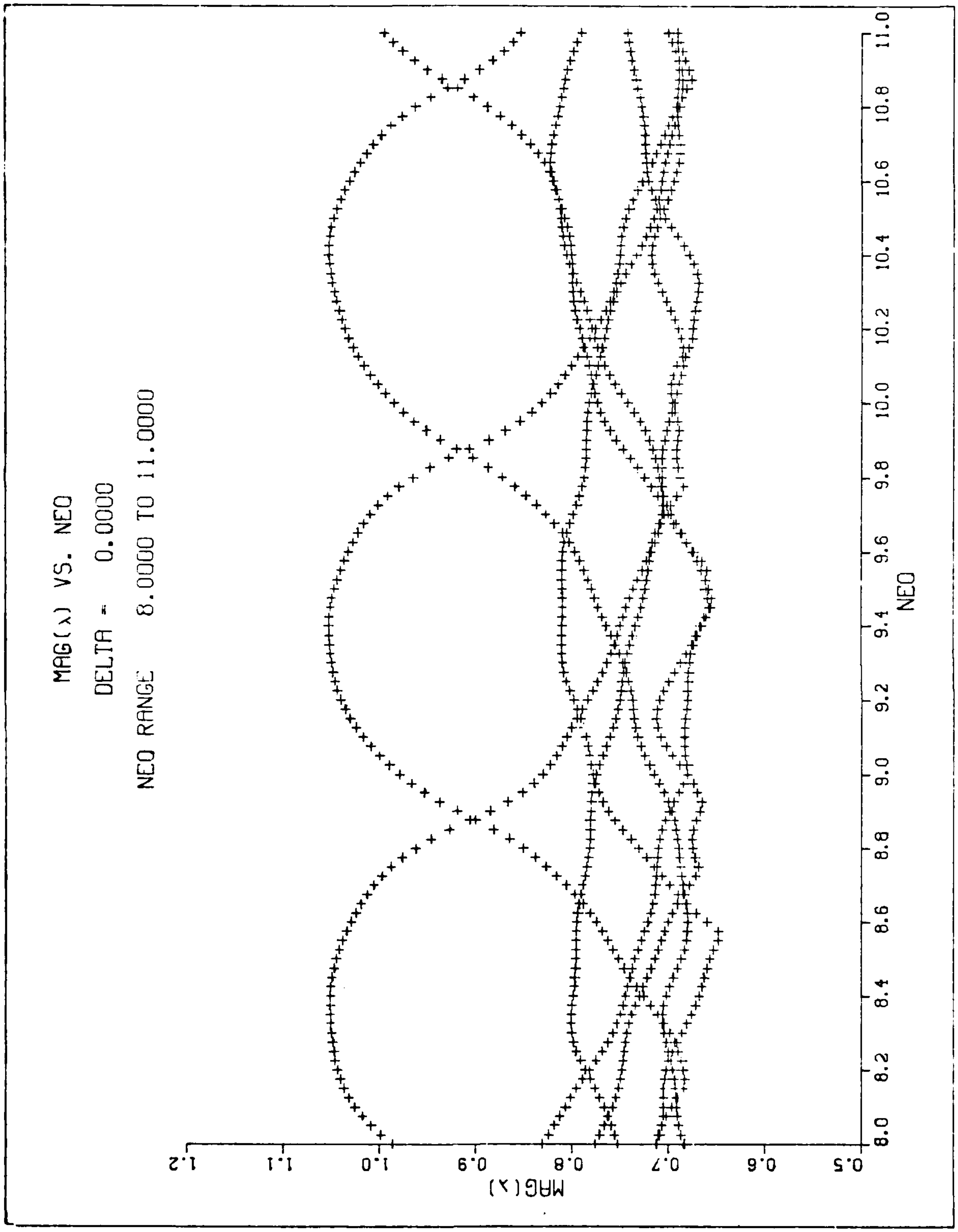

Figure 2.1. $|\lambda|$ vs N_{eq} for $8.0 \le N_{eq} \le 11.0$
The first seven (symmetric and anti-symmetric) mode eigenvalues are plotted.

Below some critical equivalent Fresnel number, $N_{eq(crit)}$, the first and second symmetric eigenvalues display either crossing or cusping at the mode separation minima points. Above $N_{eq(crit)}$, crossing of the first two eigenvalues ceases. $N_{eq(crit)}$ is given by (Ref 9:4149):

$$N_{eq(crit)} = \frac{11.5}{(\ln M)^3} \tag{2.6}$$

Above $N_{eq(crit)}$, the overall periodicity of the eigenvalues still exists. The amplitude of the fluctuations of the magnitude of λ_1 decreases as N_{eq} increases (Ref 2: 1536).

The periodic fluctuations of $|\lambda_i|$ may be better understood if the following argument is advanced. The equivalent Fresnel number is equal to the number of half wavelengths between the edge of the output mirror and the closest point on the geometric wave inside the resonator when that wave just touches the center of the mirror (Ref 10:360). This is depicted in Figure 2-2. Of all the waves that are scattered from the edge of the mirror, that which is propagated back into the resonator along the ray direction of the outgoing geometric wave is the most important. It is focused back along the optic axis, where it can interfere with the resonator mode (Ref 11:263). As N_{eq} is changed by unity, the phase of this re-entrant ray is changed by 2π radians. Consequently, there should be

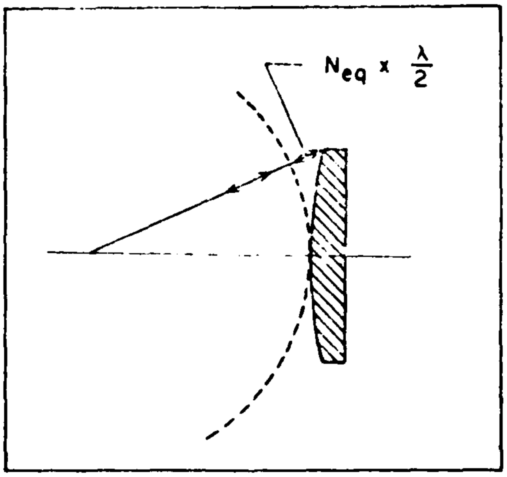

Figure 2-2. Interpretation of N_{eq} (Ref 10:360)

cyclical constructive and destructive interference along the axis, with a period of unity in N_{eq} .

Considering just the fundamental mode, when the re-entrant ray interferes destructively with the mode, the field on the resonator axis should be relatively diminished compared to the field near the edges of the mode. If the re-entrant ray interferes constructively with the mode, the field on the optic axis should be relatively more intense than the field near the edges of the mode. Hence, a resonator with N_{eq} such that destructive interference occurs should outcouple relatively more power than a resonator with N_{eq} such that constructive interference occurs.

Since the outcoupled energy of a mode is related to $|\lambda|$ as in Eq (2.3), $|\lambda|$ should also be related to the

constructive and destructive interference. When the re-entrant ray interferes constructively, $|\lambda|$ should be near its maximum. When destructive interference occurs, $|\lambda|$ should be near its minimum. Hence, for $|\lambda|$ near its maximum, the mode should be relatively built up on the resonator axis and depressed near its edges. When $|\lambda|$ is near a minimum value, the mode should be depressed on the optic axis and built up near its edges.

An examination of the fundamental mode for $5 < N_{eq} < 21$ confirms the above. $|\lambda_1|$ reaches its peak value when $N_{eq} \cong n + \frac{3}{8}$ $(n=0,1,2,...)$, and its minimum value when $N_{eq} \cong n + \frac{7}{8}$. The fundamental mode does have a depressed intensity on axis when $N_{eq} \cong n + \frac{7}{8}$ and relative intensity peaks on axis when $N_{eq} \cong n + \frac{3}{8}$. Figures 2-3 and 2-4 show representative plots of this behavior.

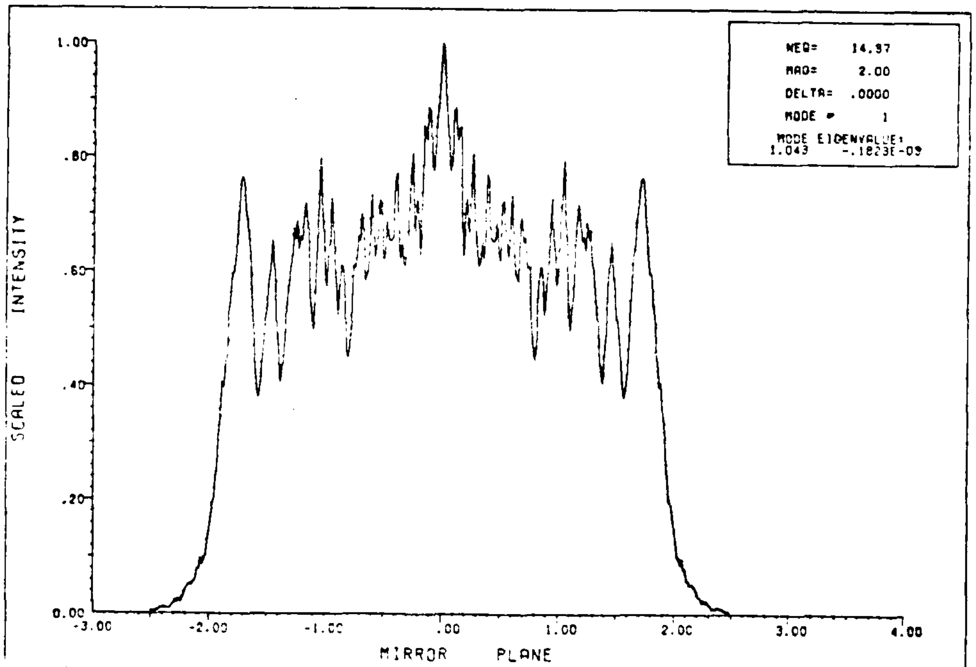

Fig. 2-3. Fundamental Mode Intensity for N_{eq}=14.37 with δ=0.0

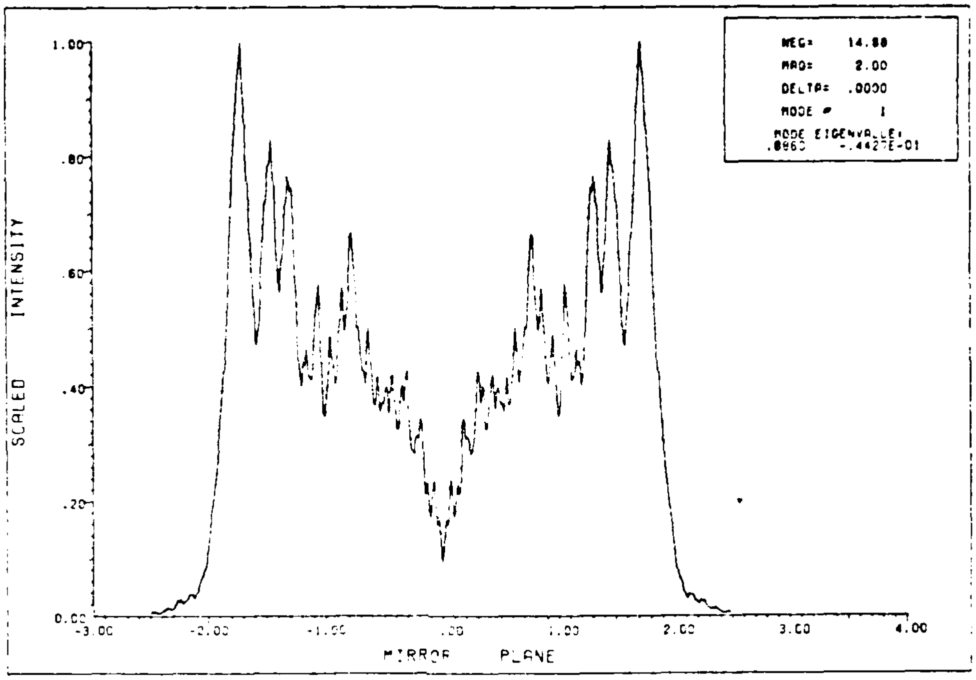

Fig. 2-4. Fundamental Mode Intensity for N_{eq}=14.8825 with δ=0.0

The Polynomial Eigenvalue Equation

The stationary phase approximation to the integral equation results in the expression

$$\lambda\{1 + \sum_{n=1}^{N} [a_n F_n(x) + b_n G_n(x)]\} = 1 + F_1(x) + G_1(x)$$

$$+ \sum_{n=1}^{N} [a_n F_{n+1}(x) + b_n G_{n+1}(x)]$$

$$+ F_1(x) \sum_{n=1}^{N} [a_n F_n(\beta) + b_n G_n(\beta)]$$

$$+ G_1(x) \sum_{n=1}^{N} [a_n F_n(\alpha) + b_n G_n(\alpha)] \tag{2.7}$$

With the manipulations detailed below, Eq (2.7) can be reduced to a polynomial in λ of order $2N+1$. The polynomial can be numerically solved for the $2N+1$ eigenvalues.

The initial step is to equate the constants and the coefficients of F_n and G_n on both sides of Eq (2.7). Equating the constants yields

$$\lambda = 1 + a_N F_{N+1} + b_N G_{N+1} \tag{2.8}$$

F_{N+1} and G_{N+1} are essentially constant, as may be seen in Eqs (1.10) and (1.11).

Equating the coefficients of $F_1(x)$ and $G_1(x)$ gives

$$\lambda a_1 = 1 + \sum_{n=1}^{N} [a_n F_n(\beta) + b_n G_n(\beta)] \tag{2.9a}$$

$$\lambda b_1 = 1 + \sum_{n=1}^{N} [a_n F_n(\alpha) + b_n G_n(\alpha)] \tag{2.9b}$$

Finally, equating the coefficients of $F_n(x)$ and $G_n(x)$, $n \neq 1$, yields

$$\lambda a_{n+1} = a_n \tag{2.10a}$$

$$\lambda b_{n+1} = b_n \tag{2.10b}$$

From Eq (2.10a),

$$a_{n+1} = \frac{a_n}{\lambda} = \frac{a_1}{\lambda^n} \tag{2.11}$$

Changing the subscripts slightly, and using Eq (2.11) twice yields

$$a_N = \frac{a_1}{\lambda^{N-1}} = \frac{a_n \lambda^{n-1}}{\lambda^{N-1}} \tag{2.12}$$

$$= a_n \lambda^{n-N} \tag{2.13}$$

Similarly,

$$b_N = b_n \lambda^{n-N} \tag{2.14}$$

Using Eqs (2.13) and (2.14), Eq (2.9) reduces to

$$a_N \lambda^N = 1 + \sum_{n=1}^{N} \lambda^{N-n} \left[a_N F_n(\beta) + b_N G_n(\beta) \right] \tag{2.15a}$$

$$b_N \lambda^N = 1 + \sum_{n=1}^{N} \lambda^{N-n} \left[a_N F_n(\alpha) + b_N G_n(\alpha) \right] \tag{2.15b}$$

Following Reference 3, define

$$F_\alpha = \sum_{n=1}^{N} \lambda^{N-n} F_n(\alpha) \tag{2.16a}$$

$$F_\beta = \sum_{n=1}^{N} \lambda^{N-n} F_n(\beta) \tag{2.16b}$$

$$G_\alpha = \sum_{n=1}^{N} \lambda^{N-n} G_n(\alpha) \tag{2.16c}$$

$$G_\beta = \sum_{n=1}^{N} \lambda^{N-n} G_n(\beta) \tag{2.16d}$$

Substitution of Eq (2.16) into Eq (2.15) and factoring out the constants a_N and b_N gives

$$a_N \lambda^N = 1 + a_N F_\beta + b_N G_\beta \tag{2.17a}$$

$$b_N \lambda^N = 1 + a_N F_\alpha + b_N G_\alpha \tag{2.17b}$$

Solving Eqs (2.17a) and (2.17b) simultaneously results in

$$a_N = \frac{G_\beta - G_\alpha + \lambda^N}{\lambda^{2N} - \lambda^N (F_\beta + G_\alpha) + F_\beta G_\alpha - F_\alpha G_\beta} \tag{2.18a}$$

$$b_N = \frac{F_\alpha - F_\beta + \lambda^N}{\lambda^{2N} - \lambda^N (F_\beta + G_\alpha) + F_\beta G_\alpha - F_\alpha G_\beta} \tag{2.18b}$$

After substituting Eqs (2.18a) and (2.18b) into Eq (2.8) and rearranging the terms, the final expression in λ is

$$\lambda^{2N+1} - \lambda^{2N} - \lambda^{N+1}(F_\beta + G_\alpha) + \lambda^N(F_\beta - F_{N+1} + G_\alpha - G_{N+1})$$

$$+ \lambda(F_\beta G_\alpha - F_\alpha G_\beta) + (F_\alpha G_\beta - F_\beta G_\alpha)$$

$$+ F_{N+1}(G_\alpha - G_\beta) - G_{N+1}(F_\alpha - F_\beta) = 0 \tag{2.19}$$

Equation (2.19) is the desired polynomial expression in λ . Note that F_α , F_β , G_α , and G_β are all polynomial functions of λ . All coefficients of λ in Eq (2.19) can be calculated, and the 2N+1 values of λ can be evaluated numerically.

Edge Effects and Decentered Resonators

When the feedback mirror M_2 of the resonator is decentered, two equivalent Fresnel numbers can be defined for the cavity. For an aligned (non-decentered) resonator, Eq (1.2) defines the N_{eq} as

$$N_{eq} = \left(\frac{a_2^2}{2\lambda' L g_1}\right) \frac{1}{2} \left(M - \frac{1}{M}\right) \tag{2.20}$$

Referring to Figure 1-2, one equivalent Fresnel number can be defined for the section of M_2 extending above the optic axis, and one for that below the optic axis. Thus,

$$N_{eq,U} = \frac{[(1+\delta)a_2]^2}{2\lambda' Lg_1} \frac{1}{2} (M - \frac{1}{M}) \tag{2.21}$$

$$= (1+\delta)^2 N_{eq} \tag{2.22}$$

Similarly,

$$N_{eq,L} = (1-\delta)^2 N_{eq} \tag{2.23}$$

The subscripts U and L refer to the upper and lower sections of M_2 .

Drawing an analogy to the aligned resonator case, the edge effects would be expected to influence the separation of $|\lambda_1|$ and $|\lambda_2|$ when $N_{eq,U}$ and $N_{eq,L}$ equal $n + \frac{3}{8}$ or $n + \frac{7}{8}$, n=0,1,2,... As δ increases from zero to unity, $N_{eq,U}$ and $N_{eq,L}$ are swept through a number of such points.

The values of δ for which the edge effects should alter the eigenvalue separation are easily determined. Starting with $N_{eq,L}$,

$$N_{eq,L} = \frac{3}{8} + \frac{K}{2} \tag{2.24}$$

where

$$K = \begin{cases} 0,2,4,\ldots & \text{for maximum mode separation} \\ 1,3,5,\ldots & \text{for minimum mode separation} \end{cases} \qquad (2.25)$$

$$(1-\delta)^2 N_{eq} = \frac{3}{8} + \frac{K}{2} \qquad (2.26)$$

$$\delta(K) = 1 - \left[\frac{\frac{3}{4} + K}{2\ N_{eq}}\right]^{\frac{1}{2}} \qquad (2.27)$$

Equation (2.27) is identical to Eqs (11) and (12) of Reference 6.

Similarly, for $N_{eq,U}$,

$$N_{eq,U} = \frac{3}{8} + \frac{K'}{2} + \mathrm{INT}(N_{eq}) \qquad (2.28)$$

where

$$K' = \begin{cases} 0,2,4,\ldots & \text{for maximum mode separation} \\ 1,3,5,\ldots & \text{for minimum mode separation} \end{cases} \qquad (2.29)$$

and where $\mathrm{INT}(N_{eq})$ is the integer portion of N_{eq} . With a little rearranging,

$$\delta(K') = \left[\frac{\mathrm{INT}(N_{eq}) + (\frac{3}{8} + \frac{K'}{2})}{N_{eq}}\right]^{\frac{1}{2}} - 1 \qquad (2.30)$$

K and K' can only assume integer values in Eqs (2.27) and (2.30).

$\delta(K)$ and $\delta(K')$ are specific, calculated values of the variable δ at which the separation between $|\lambda_1|$ and $|\lambda_2|$ should be maximal and minimal. $N_{eq,L}$ might play the dominant role in determining the shape of the eigenvalue curves as functions of δ, especially at large values of δ. As δ approaches unity, $N_{eq,L}$ becomes much smaller than $N_{eq,U}$. As noted earlier, studies of aligned resonators show that the depth of the cusps of $|\lambda_1|$ decreases as N_{eq} is increased beyond $N_{eq(crit)}$. Consequently, for large decenters, $N_{eq,L}$ may play the dominant role in determining the structure of the eigenvalue curves.

The particular importance that $N_{eq,L}$ has on the shape of the eigenvalue curves has been reported by Weiner (Ref 6: 1830-1). From Figure 2 of Reference 8, $\delta(K)$ correlates well with the δ values at which maximum and minimum separations occur between $|\lambda_1|$ and $|\lambda_2|$. No correlation between $\delta(K')$ and the separation fluctuations is made, however.

III. Theory of Integrated Intensity and Beam Steering

A general background theory of the far field integrated intensity and beam steering is presented. General relationships between the power in a given spot size and the decenter parameter δ are discussed. The beam center is defined and a simple expression relating it to the beam steering angle is given. Particular attention is paid to a Fourier optics treatment of the geometric mode throughout this chapter.

Integrated Intensity

Integrated intensity is a measure of beam quality. The integrated intensity is the amount of power falling into a given spot or "bucket" located symmetrically about the beam center. The total beam power is often normalized to unity. The integrated intensity or "power in the bucket" is then the percentage of total power falling on the spot. Plots of the far field intensity profile and the corresponding integrated intensity vs spot size curve for $N_{eq} = 9.36$ and $\delta = 0.0$ are given in Figures 3-1 and 3-2.

A number of studies, both theoretical (Refs 6, 12) and experimental (Refs 13, 14), have examined how decentering the feedback mirror affects the integrated intensity. As δ is increased from zero to unity, the percentage of total power falling inside the first Airy

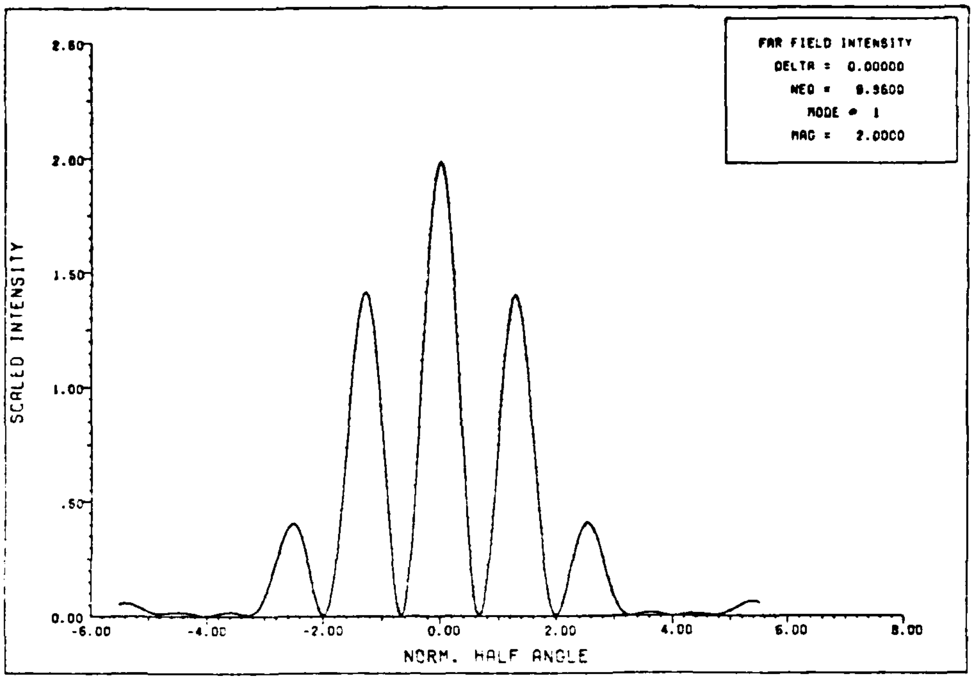

Fig. 3-1. Far Field Intensity Pattern for the Fundamental Mode with N_{eq} = 9.36 and δ = 0.0

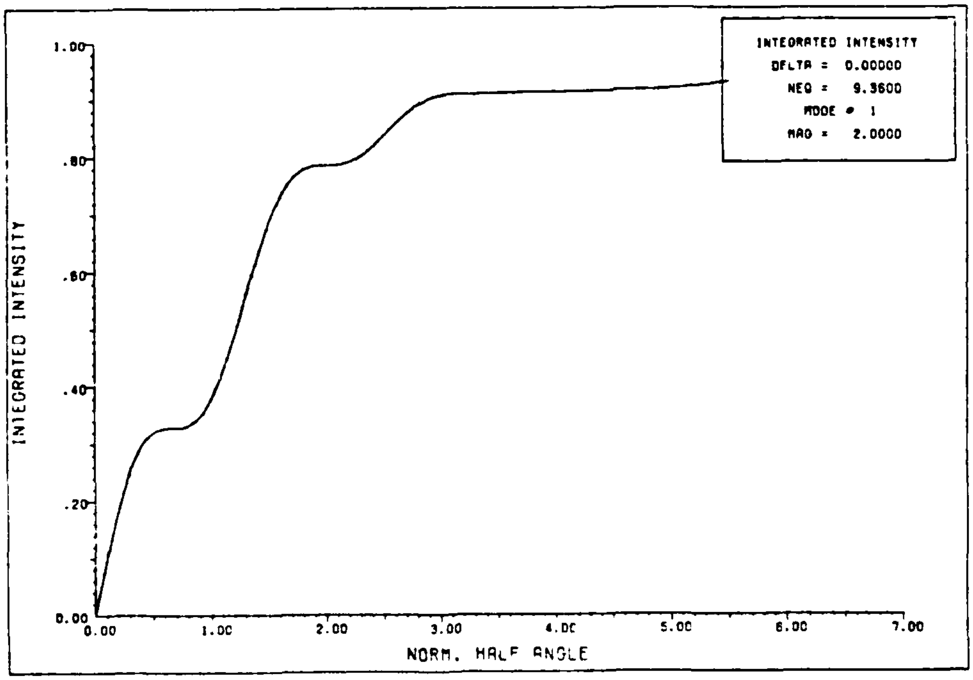

Fig. 3-2. Far Field Integrated Intensity vs Spot Size for the Mode of Figure 3-1.

disk increases monotonically for the geometric mode (Ref 12). Anen'ev et al (Ref 13) noted that the axial brightness of a Nd:YAG laser with $\delta = 1$ was much higher than that of the same laser with $\delta = 0$. The output aperture with $\delta = 1$ was effectively twice as large as that with $\delta = 0$, since the energy was extracted from a single side of the feedback mirror. Consequently, the beam divergence angle (which is proportional to the inverse of the aperture size) was reduced and the axial brightness was increased.

The far field intensity pattern for the geometric mode is derived in Appendix A. The resulting intensity $I(x_o)$ is

$$
\begin{aligned}
I(x_o) = \frac{1}{(\lambda' z)^2} \Big\{ & (M-1)^2 (1+\delta)^2 \ \mathrm{sinc}^2 \left[\frac{(M-1)(1+\delta)x_o}{\lambda' z}\right] \\
& + (M-1)^2 (1-\delta)^2 \ \mathrm{sinc}^2 \left[\frac{(M-1)(1-\delta)x_o}{\lambda' z}\right] \\
& + 2(M-1)^2 \ (1-\delta^2) \ \cos\left[\frac{2\pi(M+1)x_o}{\lambda' z}\right] \\
& \cdot \ \mathrm{sinc}\left[\frac{(M-1)(1+\delta)x_o}{\lambda' z}\right] \mathrm{sinc}\left[\frac{(M-1)(1-\delta)x_o}{\lambda' z}\right] \Big\} \qquad (3.1)
\end{aligned}
$$

where λ' is the radiation wavelength, z is the separation between the output aperture of the resonator and the obser-

vation plane, and x_o is the coordinate in the observation plane. Setting $M = 2.0$ (corresponding to the cases examined in this study) and $\delta = 0.0$, Eq (3.1) reduces to

$$I'(x_o) = \frac{2}{(\lambda' z)^2}\left[1 + \cos\left(\frac{6\pi x_0}{\lambda' z}\right)\right] \text{sinc}^2\left(\frac{x_o}{\lambda' z}\right) \tag{3.2}$$

Equation (3.2) is the far field intensity pattern for a nondecentered resonator. Setting $\delta = 1.0$, corresponding to a highly decentered resonator, the far field intensity pattern becomes

$$I''(x_o) = \left(\frac{2}{\lambda' z}\right)^2 \text{sinc}^2\left(\frac{2x_o}{\lambda' z}\right) \tag{3.3}$$

The $1 + \cos(6\pi x_o/\lambda' z)$ term in Eq (3.2) causes the energy to be spread out more than in Eq (3.3). More power will thus be deposited in a given spot for the decentered resonator $(\delta=1.0)$ than for the nondecentered resonator $(\delta=0.0)$. In fact, as δ is increased, the energy deposited in the first Airy disk increases monotonically (Fig. 3, Ref 6:1832).

The above discussion suggests that a highly decentered resonator may be capable of depositing more energy into a given spot than a nondecentered resonator. The actual resonator modes show amplitude and phase fluctuations, while the geometric mode has uniform intensity and phase profiles. However, since increasing δ changes the output aperture

from two slits to a single wider slit, the resonator modes will most likely show an increase in integrated intensity for increasing δ . This is in line with the observations of the previously cited works.

Beam Steering

The beam steering is the displacement from the optic axis that the center of the far field pattern suffers. A knowledge of the beam steering properties of a resonator is a obvious importance. Targets in the far field might be missed entirely if the beam wanders to a great degree; optical elements at the output end of the resonator might be damaged if the beam is excessively displaced from the optic axis. A particularly interesting question is how decentering the feedback mirror affects the beam steering.

The center of the beam will be defined as the centroid of the intensity profile. For a one-dimensional beam, half the power lies on either side of the centroid. Defining the center of the beam as the centroid instead of the peak intensity point can be justified by considering Figure 3-3. Although Figure 3-3 is the TEM_{10} mode of a stable resonator, the argument is the same. The intensity peaks are shifted considerably from the center of the beam, while the centroid is coincident with the center. The centroid will in general provide a better approximation of the beam center; hence, it shall be defined as the center of the beam.

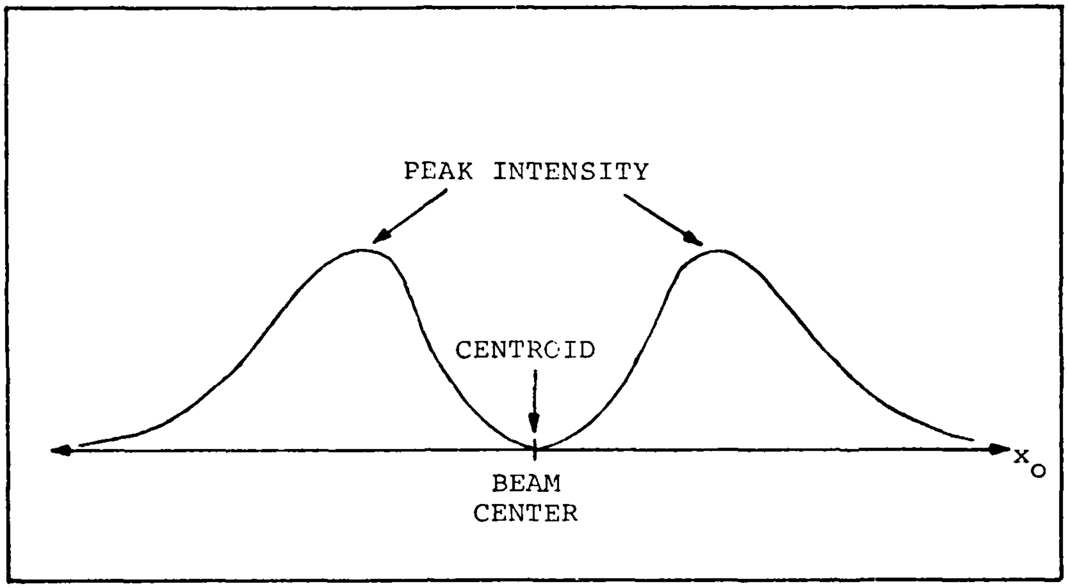

Fig. 3-3. Intensity Profile of the TEM_{10} Mode

Note that the intensity peaks are displaced from the center of the beam.

The beam steering angle θ is given by

$$\theta = \frac{x_o}{z} \tag{3.4}$$

where x_o is the location of the centroid in the observation plane. Multiplying by the dimensionless parameter $2Ma_2/\lambda'$,

$$\theta' = \frac{2Ma_2x_o}{\lambda' z} = 2Ma_2f_x \tag{3.5}$$

where f_x is the spatial frequency corresponding to the location of the centroid. Further, by setting a_2 equal

to unity, the normalized beam steering angle becomes

$$\theta_N = 2Mf_x \tag{3.6}$$

where the subscript N refers to the normalizations employed. The half-width of the central maximum of the Fraunhofer pattern of a slit of width 2M is $\theta_N = 1.0$. θ_N can thus be used to relate the beam steering angles to the radius of the Airy disk; it will be referred to as the "normalized half angle." θ_N is a very general parameter, as λ', z, and a_2 are not explicitly required for its calculation.

A major cause of beam steering is tilts on the phase of the resonator mode. If the field immediately beyond the resonator output aperture is $u(x)$, the corresponding far field pattern will be $k\,U(f_x)$, where $U(f_x)$ is the Fourier transform of $u(x)$ and k is a complex function. A linear phase tilt may be placed on $u(x)$ by multiplying $u(x)$ by $\exp(i\omega x)$. Since

$$F[u(x)e^{i\omega x}] = U(f_x - \omega/2\pi) \tag{3.7}$$

where F is the Fourier transform operator, the centroid of the far field pattern is shifted by an amount proportional to the magnitude of the phase tilt. Thus, tilted resonator modes will suffer beam steering proportional to

the sizes of the tilts.

Examination of Eq (3.1) shows that the far field intensity is an even function of x_o, regardless of M or δ. The geometric mode will, therefore, suffer no beam steering at any value of δ. The phase (as well as amplitude) profiles of resonator modes show tilts and aberrations as the resonator is decentered. The degree of phase tilting should impact the relative beam steering. If the resonator modes roughly approximate the geometric mode, the beam steering should be small. However, if the phase fronts become grossly tilted, the beam steering will be pronounced.

IV. Error Analysis of FOCAL

The computer code FOCAL propagates the resonator mode to the far field, locates the beam centroid, calculates the integrated intensity, and determines the beam steering angle. The various sources of numerical errors that enter the calculations are examined in this chapter. The errors are due to the numerical techniques and approximations employed. As it is difficult to quantify exactly the magnitudes of these errors, the following discussions will refer only to the relative sizes of the errors. A listing of the code FOCAL may be found in Appendix C.

Far Field Intensity Calculation Errors

Calculating the far field intensity requires performing a numerical Fourier transform of the resonator output field. Four primary sources of error exist in the calculation. Errors can be introduced if the mesh points of the resonator mode are too widely spaced. Inherent inaccuracies exist in the integration technique used to compute the Fourier transforms. Errors arise if the far field intensity is calculated at spatial frequencies above a certain limit. Finally, spacing the mesh points on the far field pattern too far apart will create additional discrepancies.

If the resonator mode mesh spacing is too wide, high spatial frequency information will be lost (see Figure 4-1). The field that is calculated will be a low-pass filtered, and thus inaccurate, representation of the mode. This is easily remedied by increasing the number of field points calculated, with a corresponding decrease in the mesh spacing. Unfortunately, this solution can become expensive in computer time. A reasonable compromise was made in this study by calculating the field at 100 points over the surface of the feedback mirror. Increasing the number of points from 100 did not produce a noticeable increase in mode detail. Consequently, the error introduced in the calculation of the near field pattern (resonator mode) can be considered negligible.

Rather than use one of the available fast Fourier transform (FFT) routines, an algorithm based on a numerical integration was written to perform the beam propagation. The integration technique used was Simpson's rule (Ref 15:136-138). This method connects adjacent data points with quadratic curves and sums the resultant areas. This will produce some error if the data points are not connected by quadratic functions (see Figure 4-2). A higher-order scheme, such as Weddle's rule, could have been employed. However, this would have required additional computer time, so the simpler (and less accurate) Simpson's rule was used. This probably introduced the greatest error in calculating the far field intensity.

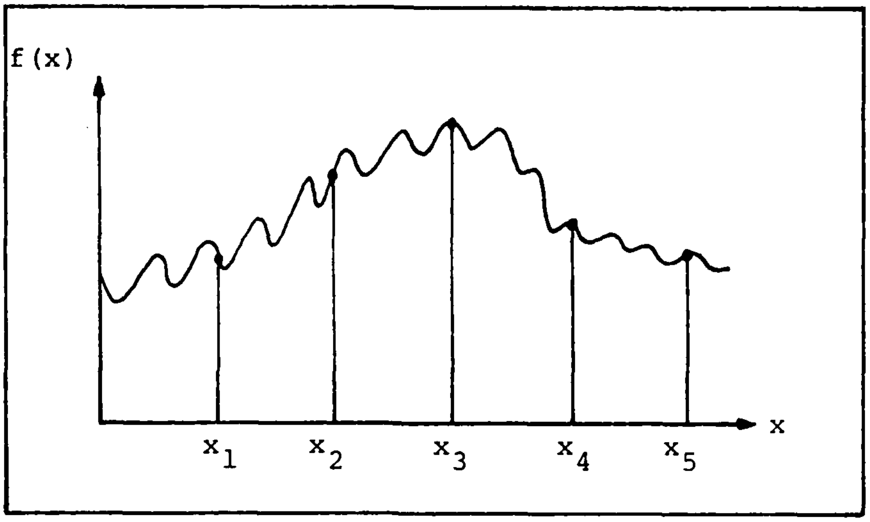

Fig. 4-1. Plot Depicting Improper Sample Spacing
Note the loss of high frequency data.

The Nyquist criterion states that a signal with a highest frequency component W can be perfectly recovered if it is sampled at a rate $f_s > 2W$ and the samples are processed by a low-pass filter (Ref 16:68-71). Using this criterion, the far field intensity can only be calculated for spatial frequencies f_x in the range

$$-\frac{1}{2T_s} \leq f_x \leq \frac{1}{2T_s} \qquad (4.1)$$

where T_s is the mesh spacing on the resonator mode. In this study, f_x was always less than $1/35T_s$. As a result, this source of error can be considered negligible.

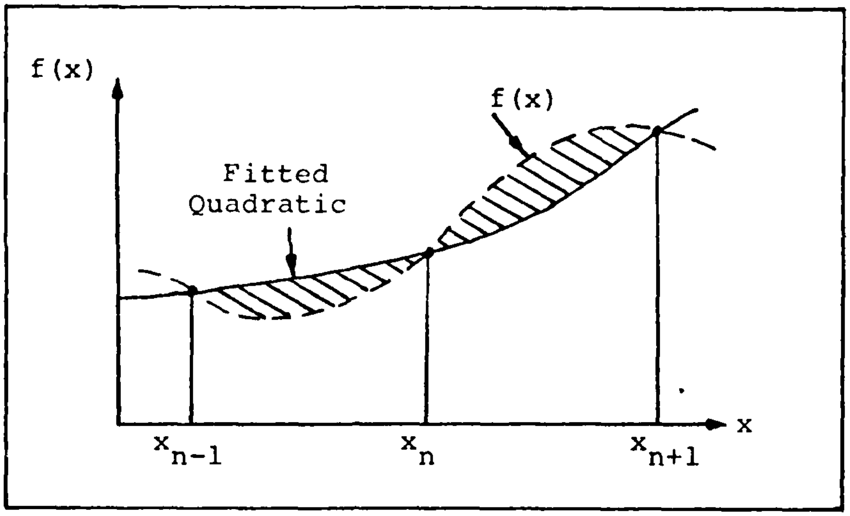

Fig. 4-2. Exaggerated Plot Showing the Discrepancy Between f(x) and a Fitted Quadratic. Error is Shaded.

The final source of error is the spacing between data points on the calculated intensity pattern. This is identical to the problem of mesh spacing on the resonator mode - a wide spacing creates loss of higher frequency data. This problem can be resolved by decreasing the data point separation. During actual runs, the far field intensity profiles were found to be quite smooth. A mesh spacing of approximately 0.06 normalized half angles (nha) was discovered to be much more than adequate to recover all of the fine detail. The errors introduced in this manner were thus quite small.

The use of Simpson's rule in the Fourier tranform routine introduced the most error into the far field intensity calculation. The other three error sources were small by comparison, and can most probably be neglected.

Errors Associated with Locating the Centroid

The centroid of the far field intensity is located in a three-step process. First, the total power P_o between two interactively-specified limits is determined by a numerical integration. Then, starting at the lower limit, the intensity is integrated until the two mesh points on either side of the half-power point are found. Finally, a linear interpolation is used to approximate the location of the centroid between the two mesh points. This suggests three main sources of error: part of the power is not used in the integration due to the finite limits imposed, the exact power cannot be determined because of problems inherent in the numerical integration, and the linear interpolation will not precisely locate the centroid.

The far field intensity pattern theoretically extends from $-\infty$ to $+\infty$. Beyond a few Airy disks from the centroid, though, the intensity becomes negligible. Since the numercial integration cannot be performed from $-\infty$ to $+\infty$, some of the power is necessarily ignored. This introduces error into the calculation, as the intensity profiles generally are not symmetric. To minimize this error, a criterion was established that at least 90% of the power must lie between the limits of integration. (This was readily determined. The power in the beam leaving the resonator was normalized to unity. As long as the power between the limits of integration was greater than 0.9, the

90% criterion was fulfilled.) In general, the power between the limits of integration ranged from 90% to 95%. This was deemed to yield sufficiently accurate results.

The use of Simpson's rule as the integration technique introduces some error into the calculation. The reasons are discussed earlier in this chapter. The far field intensity patterns were quite smooth, and 501 mesh points were used in the calculations (which roughly equates to 85 points across the Airy disk). Consequently, the errors introduced by the integration were probably small.

The linear interpolation adds further error to the calculation. This is illustrated in Figure 4-3. Point A represents the actual centroid. Point B is the "centroid" located by the interpolation. An error equal to ε thus exists.

The maximum value $|\varepsilon|$ can have is $x_{n+1} - x_n$, which is the mesh spacing. $|\varepsilon|$ could be reduced by decreasing the data point spacing. This would require additional mesh points and more computer time. During actual runs, $|x_{n+1} - x_n|$ was on the order of 0.025 nha. Decreasing the spacing beyond this limit would have required inordinate amounts of extra computer time. $|\varepsilon|$ could also be decreased by using a higher-order inverse interpolation scheme. Such a technique did not exist as a computer library routine, and the time required to create a routine was not deemed justifiable in terms of the potential returns.

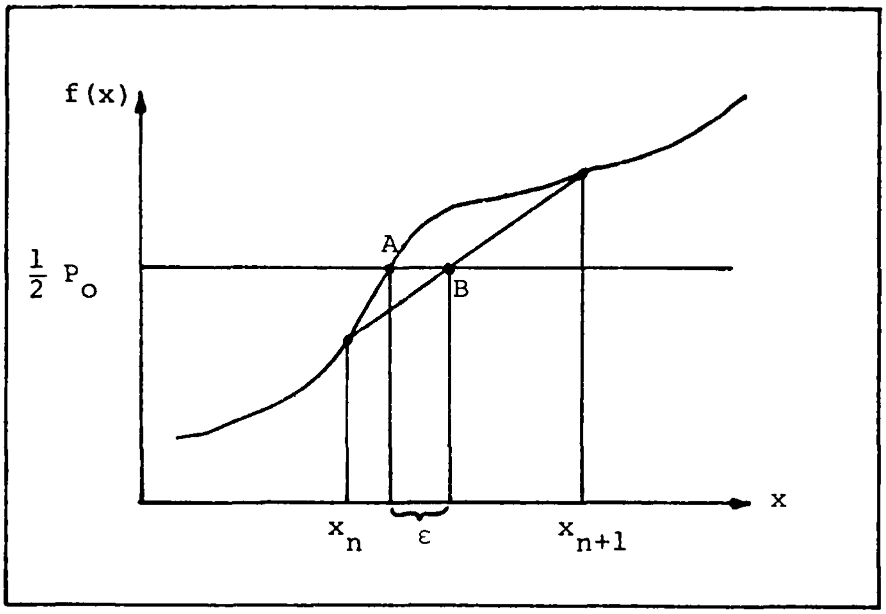

Fig. 4-3. Linear Interpolation Contribution to the Centroid Error. A is the centroid, B is the estimated centroid, and ε is the error.

A value of the "maximum error in centroid location" is printed by FOCAL. This is equal to the mesh spacing.

Three main sources of error exist in locating the centroid. It is somewhat unclear as to which introduces the greatest inaccuracy. Measures were taken to reduce the errors in all cases.

Integrated Intensity Calculation Errors

The integrated intensity is calculated in a two-step process after the centroid is located. First, the intensity profile is recomputed between symmetric limits about the centroid. Then, using Simpson's rule, the intensity is

integrated outward from the centroid to the limits. Errors enter the calculation during the location of the centroid, the computation of the intensity pattern, and the outward integration. The first two sources of error have been discussed earlier.

The third source of error is again due to the inherent problems of the numerical integration. Since the intensity patterns were relatively smooth and the mesh spacing small (0.025 nha), the inaccuracy of the integrations was minimized. Decreasing the mesh spacing further would probably have produced a small increase in accuracy for the additional expenditure of computer time.

V. Study Results

This chapter presents the results of the computer analyses of the resonator. The effects of decenters on the eigenvalues are discussed first. Next, the changes in beam quality due to decenters are presented. The chapter is concluded by examining how decenters affect the beam steering.

Effects of Decenters on the Eigenvalues

The eigenvalues were studied as functions of δ with N_{eq} a fixed parameter. The twenty-five cases examined are listed in Table I. The N_{eq} values were chosen to lie about the points of maximum and minimum separation between $|\lambda_1|$ and $|\lambda_2|$ (9.37 and 9.87, respectively) and an intermediate value (9.60). In all cases, the increment value for δ was 0.004. Typical plots are shown in Figures 5-1 through 5-6.

A note should be made concerning several conventions used. $\delta(K)$ and $\delta(K')$ refer to the δ values calculated from Eqs (2.27) and (2.30), respectively. $\delta(K \text{ even})$ refers to those values of $\delta(K)$ for which K is even. Similar remarks may be made for $\delta(K \text{ odd})$, $\delta(K' \text{ even})$, and $\delta(K' \text{ odd})$.

The eigenvalue plots were analyzed for five different items. First, the overall and fine structures were

TABLE I

Eigenvalue Analysis - Cases Examined

N_{eq}	δ Range	N_{eq}	δ Range
9.30	0.0-0.4	9.60	0.0-0.9
9.31	0.0-0.4	9.625	0.0-0.9
9.32	0.0-0.4	9.65	0.0-0.4
9.33	0.0-0.4	9.80	0.0-0.4
9.34	0.0-0.4	9.81	0.0-0.4
9.35	0.0-0.4	9.82	0.0-0.4
9.36	0.0-0.9	9.83	0.0-0.4
9.37	0.0-0.4	9.84	0.0-0.4
9.38	0.0-0.9	9.85	0.0-0.4
9.39	0.0-0.4	9.86	0.0-0.9
9.55	0.0-0.4	9.87	0.0-0.4
9.575	0.0-0.4	9.88	0.0-0.9
		9.89	0.0-0.4

correlated to $\delta(K)$ and $\delta(K')$, respectively. The crossing and cusping nature of $|\lambda_1|$ and $|\lambda_2|$ was examined in detail. Next, the separation between $|\lambda_1|$ and $|\lambda_2|$ was related to $N_{eq,U}$, $N_{eq,L}$, and δ. The interleaving of the higher-order eigenvalues was explored. Finally, crossings between $|\lambda_2|$ and $|\lambda_3|$ were examined.

Examination of Figures 5-1 through 5-6 reveals that $|\lambda_1|$ and $|\lambda_2|$ have an overall periodicity in $N_{eq,L}$. This periodicity was observed in all the cases studied. The separation between $|\lambda_1|$ and $|\lambda_2|$ exhibit maxima and minima quite close to the $\delta(K)$ values. In the six applicable cases, $\delta(K=0)$ was somewhat greater than the δ value at which the peak separation occurred.

Superimposed on the overall oscillatory structure is a fine structure periodic in $N_{eq,U}$. The structure is most pronounced for $\delta < 0.2$, where $N_{eq,U}$ is of the same order as $N_{eq,L}$. For $\delta > 0.75$, the periodicity still exists, but does not go exactly as $N_{eq,U}$.

The separation between $|\lambda_1|$ and $|\lambda_2|$ exhibits minor minima at the $\delta(K'$ odd) values. This agrees with the theory of Chapter II. At these δ values, the $|\lambda_1|$ curves are depressed and the $|\lambda_2|$ curves are peaked. The magnitudes of the depressions and peaks decrease as δ increases. The correlation between these minor minima and $\delta(K'$ odd) is excellent for $\delta < 0.7$. For $\delta > 0.7$, the correlation begins to break down.

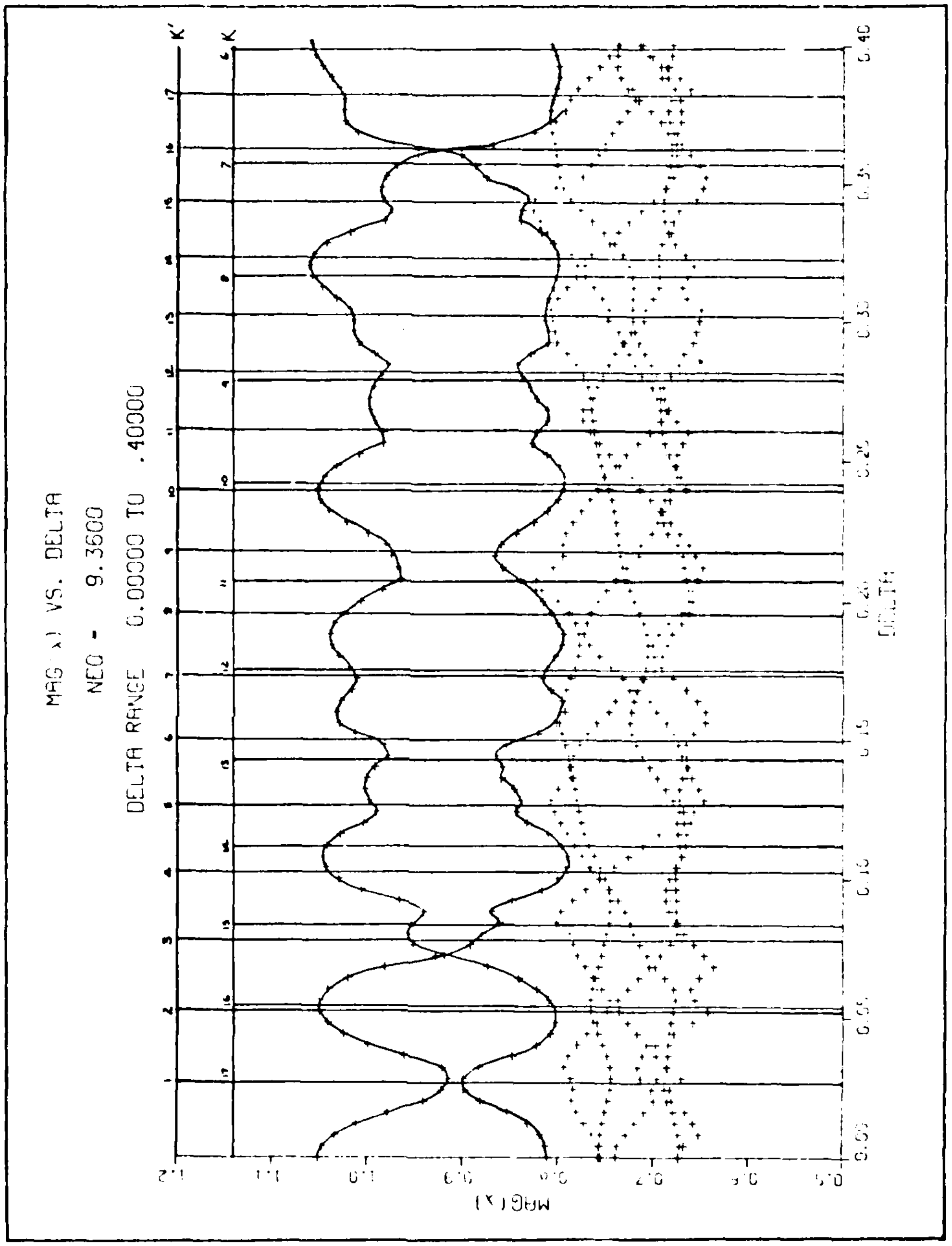

Fig. 5-1. Eigenvalue Plot for N_{eq} = 9.36, $0.0 \le \delta \le 0.4$

/

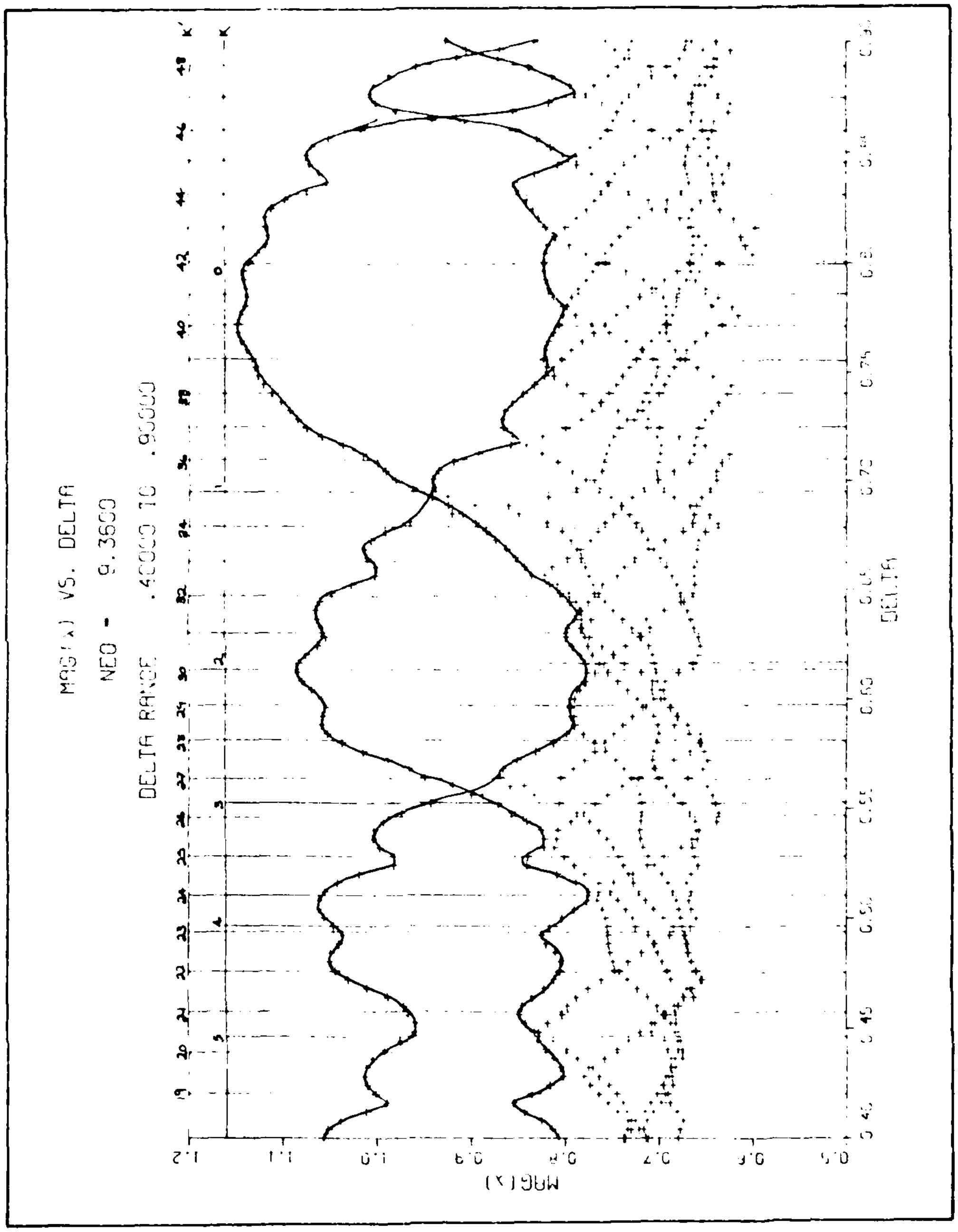

Fig. 5-2. Eigenvalue Plot for N_{eq} = 9.36, $0.4 \leq \delta \leq 0.9$

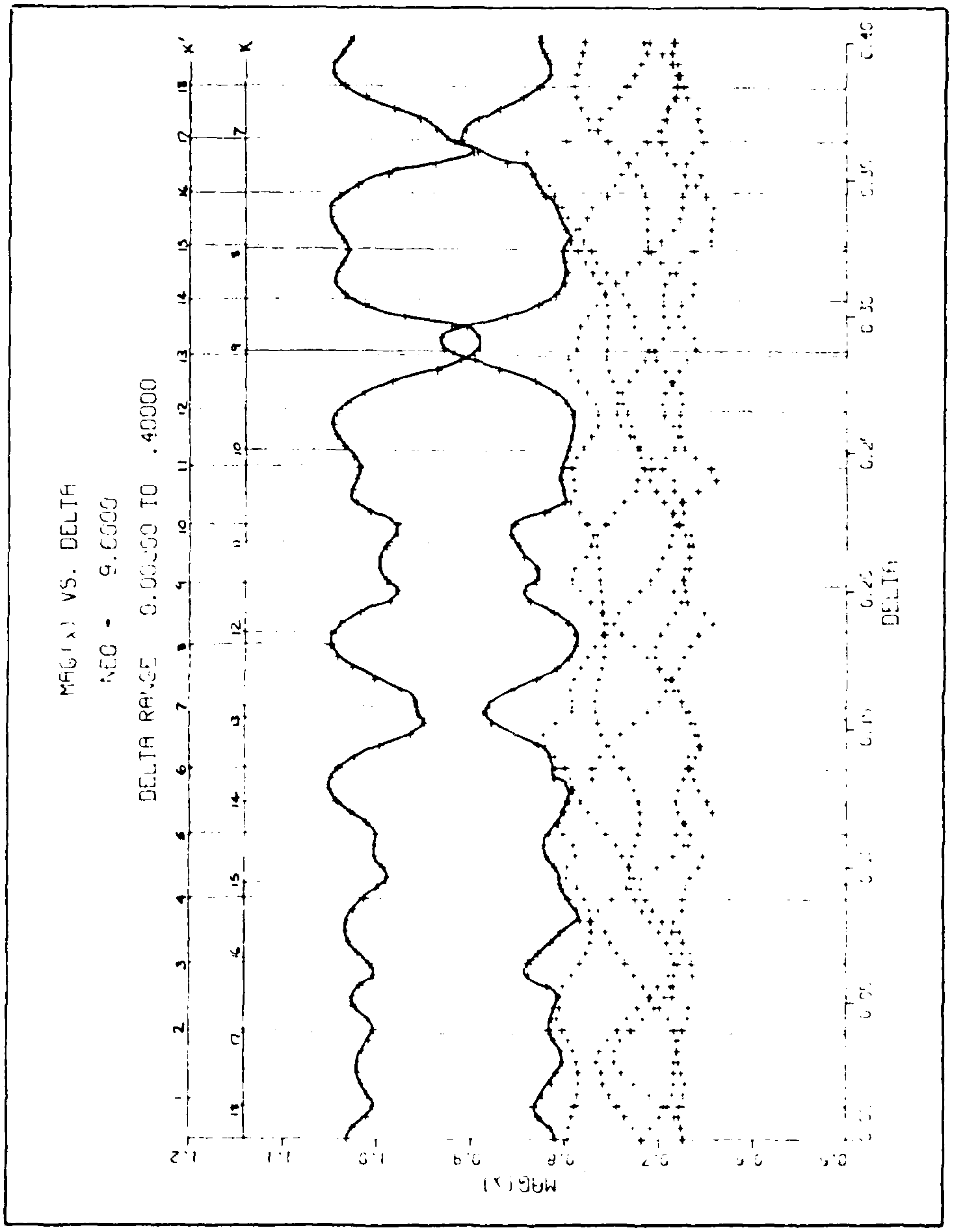

Fig. 5-3. Eigenvalue Plot for N_{eq} = 9.6, $0.0 \leq \delta \leq 0.4$

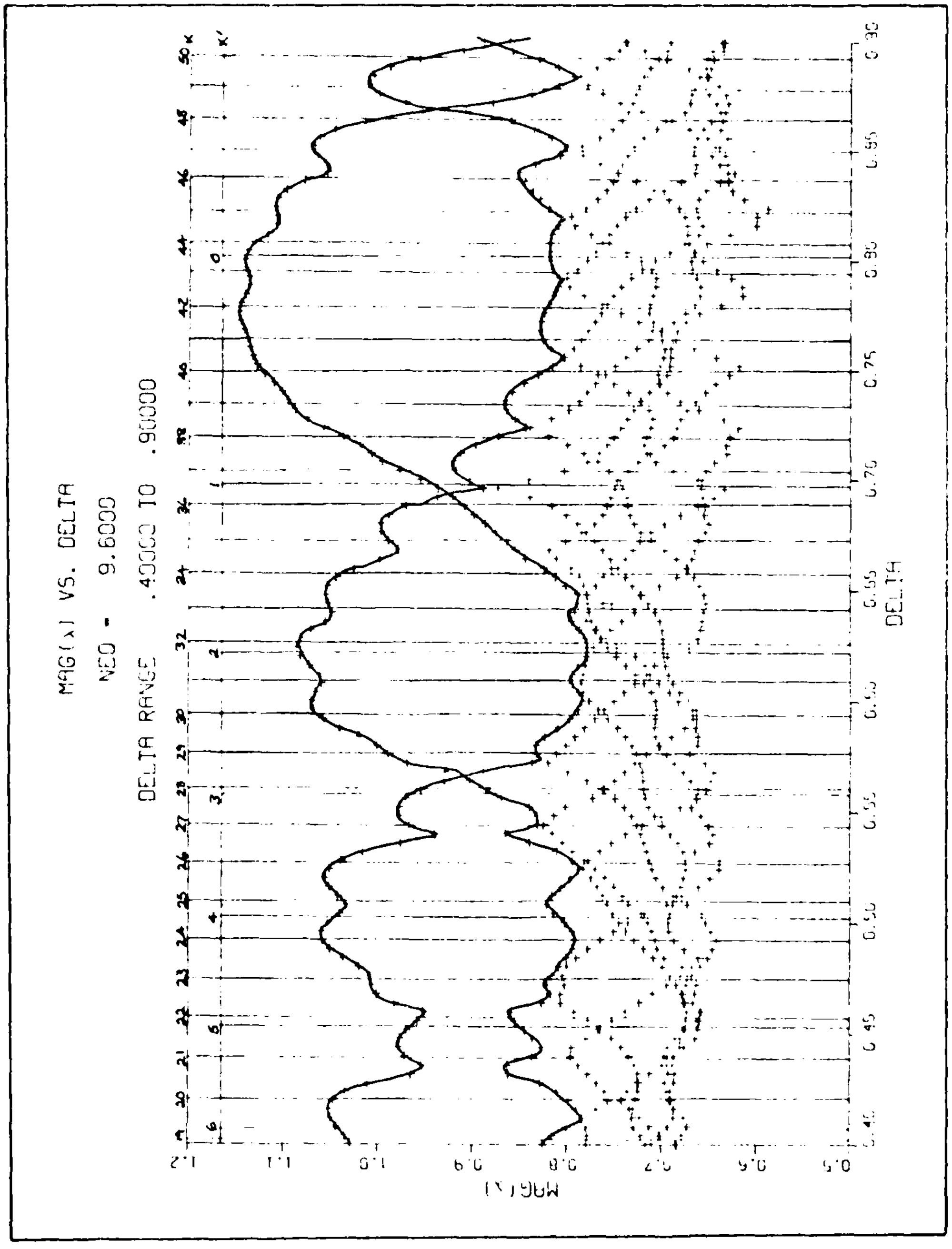

Fig. 5-4. Eigenvalue Plot for N_{eq} = 9.6, $0.4 \leq \delta \leq 0.9$

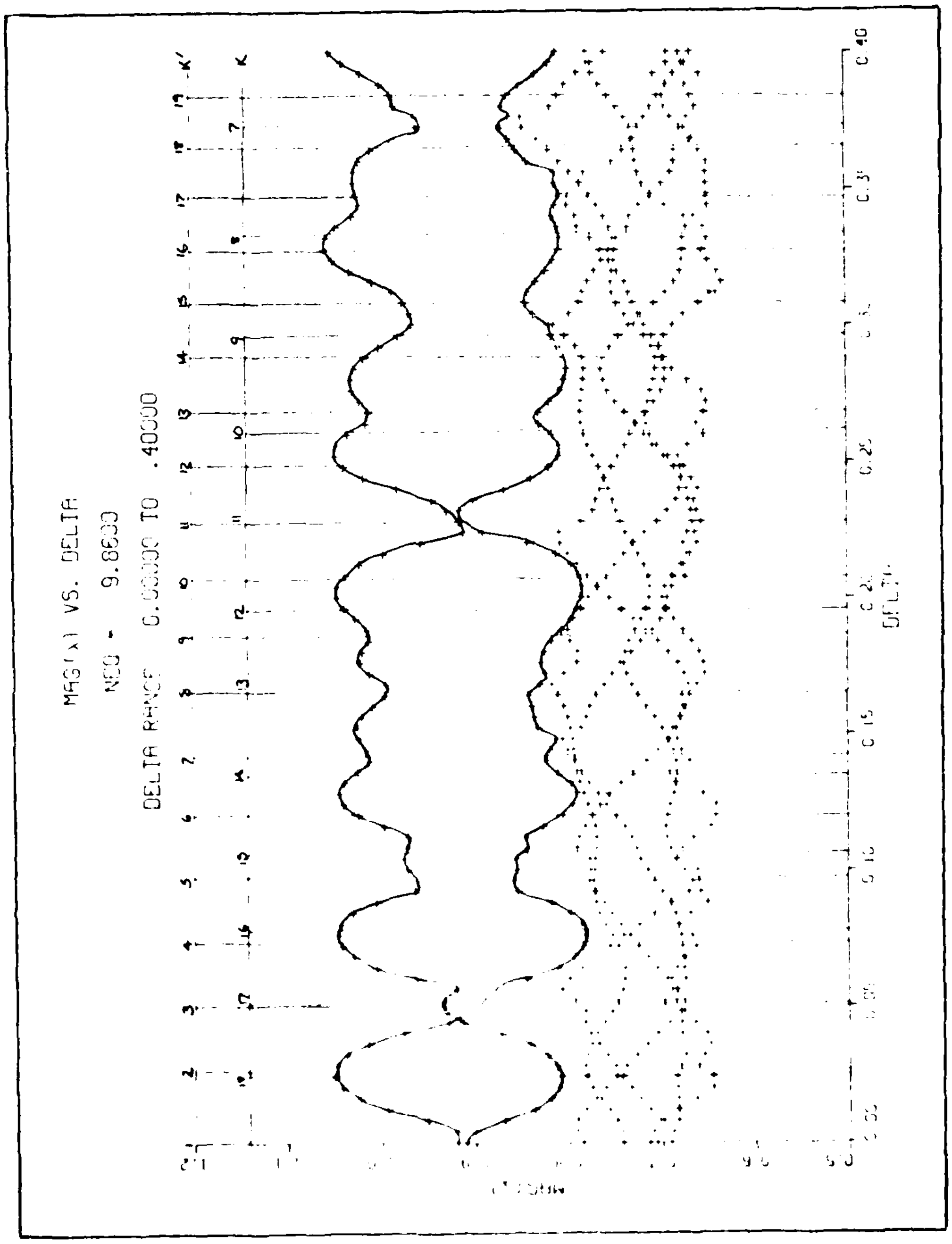

Fig. 5-5. Eigenvalue Plot for N_{eq} = 9.86, $0.0 \leq \delta \leq 0.4$

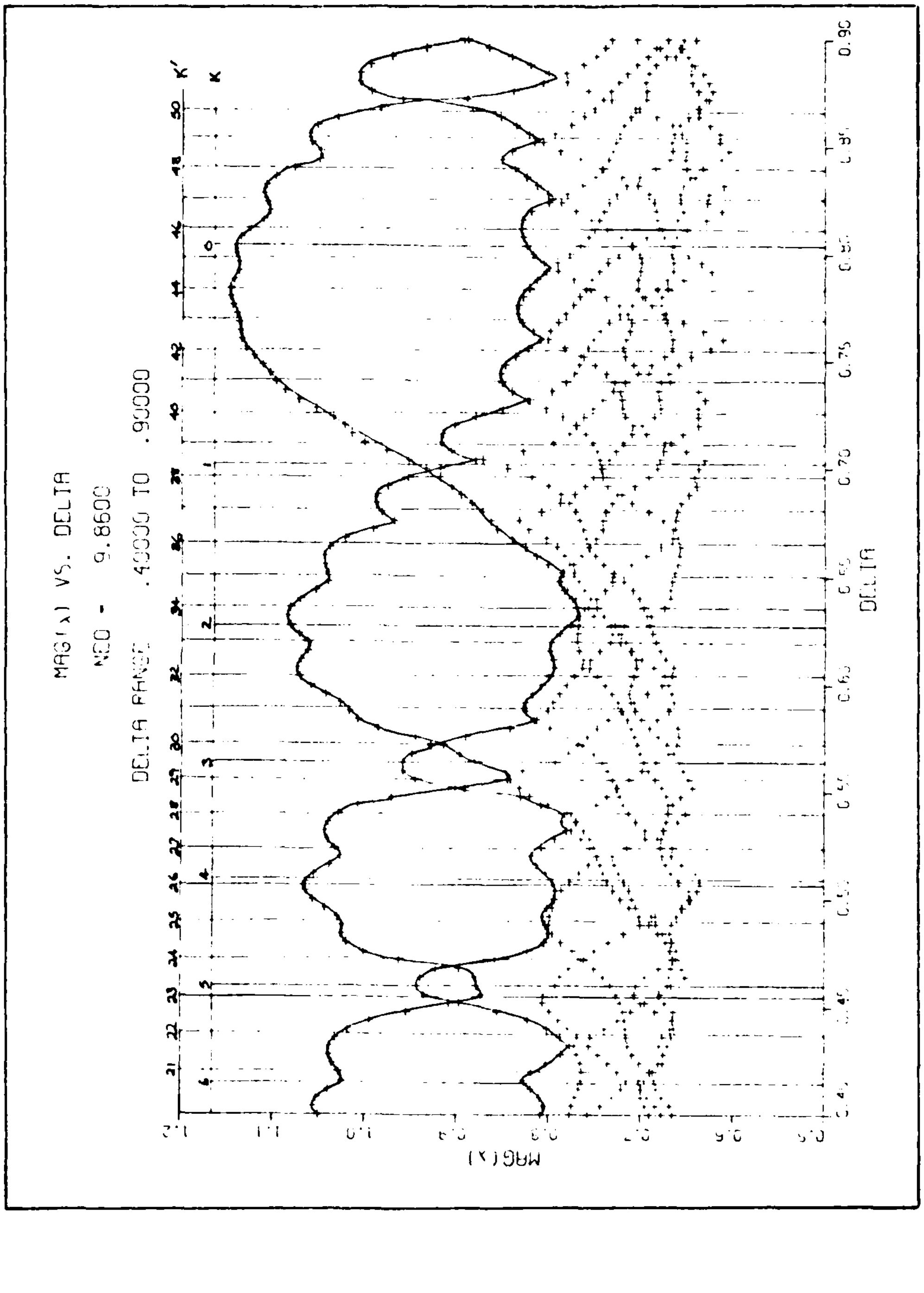

Fig. 5-6. Eigenvalue Plot for N_{eq} = 9.86, $0.4 \le \delta \le 0.9$

At the $\delta(K'$ even) values, two distinct types of behavior are observed for $|\lambda_1|$ and $|\lambda_2|$. In the first type of behavior, a minor separation peak is observed. Alternatively, both the $|\lambda_1|$ and $|\lambda_2|$ curves exhibit very steep slopes of opposite sign. The slopes of the curves in these regions are considerably greater than the slopes in the surrounding neighborhoods. Even though separation peaks are not exhibited, the curves appear to be "stretched apart," thus creating the steep slopes. This form of behavior occurred more often than the other. The correlation between the two types of behavior and $\delta(K'$ odd) is excellent for $\delta < 0.7$. For $\delta > 0.7$, the correlation begins to break down.

Prominent cusps or mode crossings between $|\lambda_1|$ and $|\lambda_2|$ exist at almost all $\delta(K$ odd) values. Weiner (Ref 6: 1831) asserts that at moderately large N_{eq} values (comparable to those used in this study), the first crossover points do not occur until δ is relatively large. In this study, crossings were observed for δ as low as 0.01 (N_{eq} = 9.88, 9.89). Cusping can - and usually does - occur when δ is increased from the first crossing point. Only crossing behavior is observed for $\delta > 0.5$.

The $\delta(k$ odd) cusps evolve in a regular manner as N_{eq} is increased. The four major stages of the cyclic behavior are displayed in Figure 5-7. $N_{eq,U}$ and $N_{eq,L}$ play important roles in the evolutionary cycle.

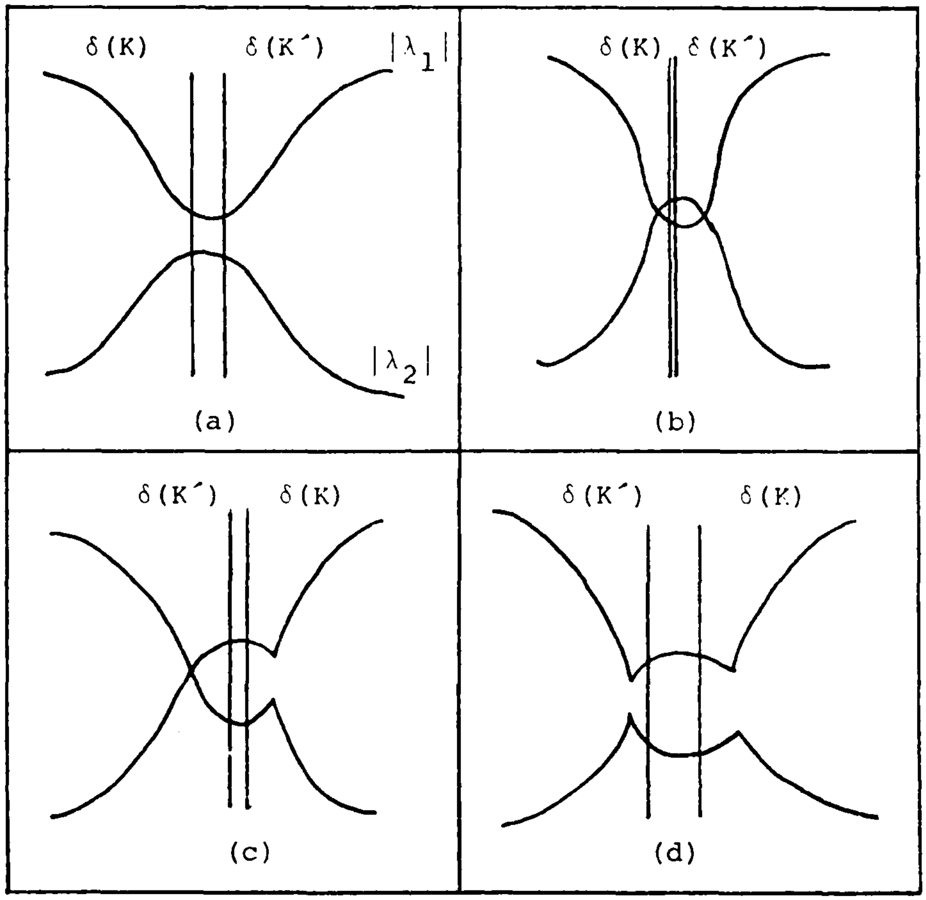

Fig. 5-7. Life Cycle of a Major Cusp

(a) First Stage; (b) Second Stage; (c) Third Stage; (d) Fourth Stage

In the first stage of the cycle, a deep cusp forms at a pair of $\delta(K \text{ odd})$ and $\delta(K' \text{ odd})$ values that are approximately equal. Invariably, $\delta(K \text{ odd}) < \delta(K' \text{ odd})$. As N_{eq} is increased, $\delta(K \text{ odd})$ and $\delta(K' \text{ odd})$ become almost equal, and the cusp deepens. In the second stage, $\delta(K \text{ odd})$ is virtually equal to $\delta(K' \text{ odd})$. The cusp exhibits two mode degeneracy points. As N_{eq} is further increased, the third stage is entered. $\delta(K \text{ odd})$ becomes larger than $\delta(K' \text{ odd})$, and one of the degenerate points breaks open. At this stage, the cusp has evolved into a single mode crossing. In the fourth stage, $\delta(K \text{ odd})$ and $\delta(K' \text{ odd})$ are somewhat separated. The remaining mode degeneracy breaks open, and the eigenvalues completely separate. As N_{eq} is increased further, the mode separation becomes greater until no cusping nature is evident. What was once a cusp has evolved into a region of relatively large mode separation. This evolutionary behavior was observed in virtually all cusps corresponding to $\delta(K \text{ odd})<0.4$.

The separation between $|\lambda_1|$ and $|\lambda_2|$ is a function of $N_{eq,U}$, $N_{eq,L}$, and δ. Several distinctive types of behavior may be observed.

If K and K' are of the same parity, several pairs of $\delta(K)$ and $\delta(K')$ are approximately equal, and if $\delta < 0.15$, then the mode separation is characterized by rapid, deep oscillations. This behavior is observed near N_{eq} = 9.37 and 9.87. In these regions, the cusps are quite deep

and often doubly degenerate. Mode crossings occasionally occur. The mode separation is quite unstable and changes rapidly for small changes of δ . The behavior suggests that the edge waves from both edges of the feedback mirror reinforce each other, thus creating the large oscillations in $|\lambda_1|$ and $|\lambda_2|$.

If K and K' are of the opposite parity, several pairs of $\delta(K)$ and $\delta(K')$ values are approximately equal, and if $\delta < 0.15$, then the mode separation remains roughly constant at an intermediate value. This behavior may be observed near $N_{eq} = 9.625$. In these regions, changes in δ produce minor changes in the separation between $|\lambda_1|$ and $|\lambda_2|$. It appears that the edge waves from both edges of the feedback mirror interfere destructively with each other. Each wave nulls out the effects of the other. Consequently, the oscillatory behavior is suppressed, and the mode separation remains roughly constant.

The greatest mode separation occurs for $\delta \cong 0.8$, near $\delta(K = 0)$. The separation stability is quite good near $\delta = 0.8$: $\frac{d}{d\delta}(|\lambda_1|-|\lambda_2|)$ is rather small. For $\delta > 0.3$, the separation of the peaks of the overall oscillatory structure increases with δ . A comparison of the mode separations for $\delta \cong 0.0$ and $\delta \cong 0.8$ is given in Table II. The separations show improvements of 38% to 51% when the resonator is highly decentered. This agrees with the observations of Weiner (Ref 6:1831).

TABLE II

Comparison of Eigenvalue Separation

N_{eq}	δ*	$\|\lambda_1\|$	$\|\lambda_2\|$	$\Delta\lambda$**	Δ%***
9.36	0.0	1.0515	0.8107	0.2408	42.4
9.36	0.776	1.1437	0.8007	0.3430	
9.38	0.0	1.0519	0.8105	0.2414	41.7
9.38	0.776	1.1416	0.7996	0.3420	
9.60	0.0	1.0318	0.8096	0.2222	47.0
9.60	0.792	1.1352	0.8085	0.3267	
9.625	0.0	1.0272	0.8079	0.2193	51.2
9.625	0.788	1.1363	0.8048	0.3315	
9.86	0.024	1.0495	0.8087	0.2408	38.4
9.86	0.792	1.1368	0.8035	0.3333	
9.88	0.024	1.0502	0.8075	0.2427	38.8
9.88	0.792	1.1372	0.8002	0.3369	

* δ values listed correspond to the maximum $\Delta\lambda$ values nearest δ=0.0 or K=0.

** $\Delta\lambda = |\lambda_1| - |\lambda_2|$

*** $$\Delta\% = \frac{\Delta\lambda_{K\cong 0} - \Delta\lambda_{\delta\cong 0}}{\Delta\lambda_{\delta\cong 0}} \cdot 100$$

The eigenvalue magnitudes of the higher-order modes interleave with and cross one another. The interleaving is somewhat regular for $\delta < 0.6$, but no periodicity in $N_{eq,U}$, $N_{eq,L}$, or δ can be readily discerned. Some modes appear to meander with no apparent periodicity for $\delta < 0.6$. For $\delta > 0.6$, the periodicity is much more pronounced. The "meandering modes" generally cease to exist, leaving only a diamond-shaped interleaving pattern. The pattern is roughly periodic in $N_{eq,U}$.

Crossings between $|\lambda_2|$ and $|\lambda_3|$ occur at all values of δ . For $\delta < 0.4$, the mode crossings are sporadic and aperiodic. For $0.4 < \delta < 0.65$, the crossings are more frequent. For $\delta > 0.65$, the crossings are quite regular and approximately periodic in $N_{eq,U}$.

In summary, the eigenvalues exhibit an overall and a fine structure periodic in $N_{eq,L}$ and $N_{eq,U}$, respectively. $\delta(K)$ and $\delta(K')$ correlate very well to the maximum and minimum separation points of $|\lambda_1|$ and $|\lambda_2|$. The cusps at the δ(K odd) values show a cyclic behavior in N_{eq} . The separation between the first two eigenvalues is apparently influenced by the edge waves from the feedback mirror. The maximum separation of these two eigenvalues occurs near $\delta = 0.8$; the peaks in the separation increase in magnitude as δ increases. Finally, the higher-order eigenvalues display a periodic interleaving for large δ values.

Effects of Decenters on Beam Quality

The far field integrated intensity of the first four modes was examined for decentered resonators with equivalent Fresnel numbers of 9.36, 9.625, and 9.86. δ ranged from 0.0 to 0.9 in increments of 0.05. Specifically, the power deposited within one, two, and three Airy disks (normalized half angles) of the optic axis was calculated. The number of Airy disks required to capture 90% of the power was also computed. Plots of the results for $N_{eq} = 9.36$ are shown in Figures 5-8 through 5-15. Each plot shows the results for the geometric mode and either modes one and two or modes three and four.

The plots were examined for five specific items. First, general increasing or decreasing trends of the data with δ were observed. Second, the modes were compared to determine if any mode had consistently better beam quality than the others. The same comparisons were then made between the four resonator modes and the geometric mode. Next, the percent differences of the integrated intensity for $\delta = 0.0$ and $\delta = 0.8$ were calculated. Finally, the range of δ values for which the beam quality was the best (most power deposited in a given spot size) was determined.

The integrated intensity of the geometric beam is dependent on δ . The power deposited in one Airy disk increases monotonically as δ is increased. This agrees with results published in the literature (Ref 12). The power in two Airy

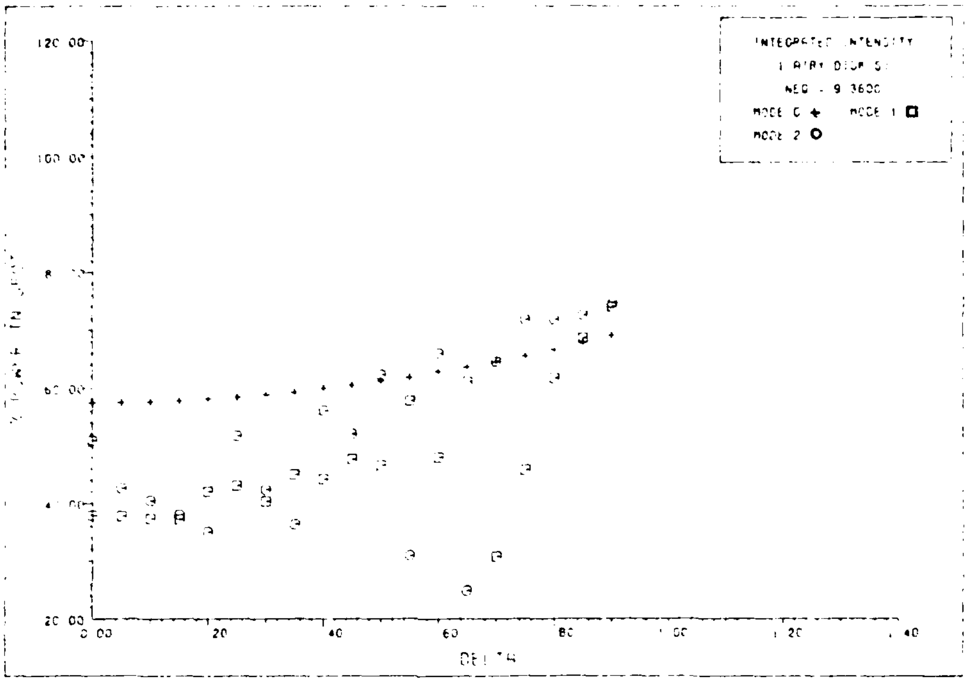

Fig. 5-8. Integrated Intensity in One Airy Disk for Modes One and Two. $N_{eq} = 9.36$

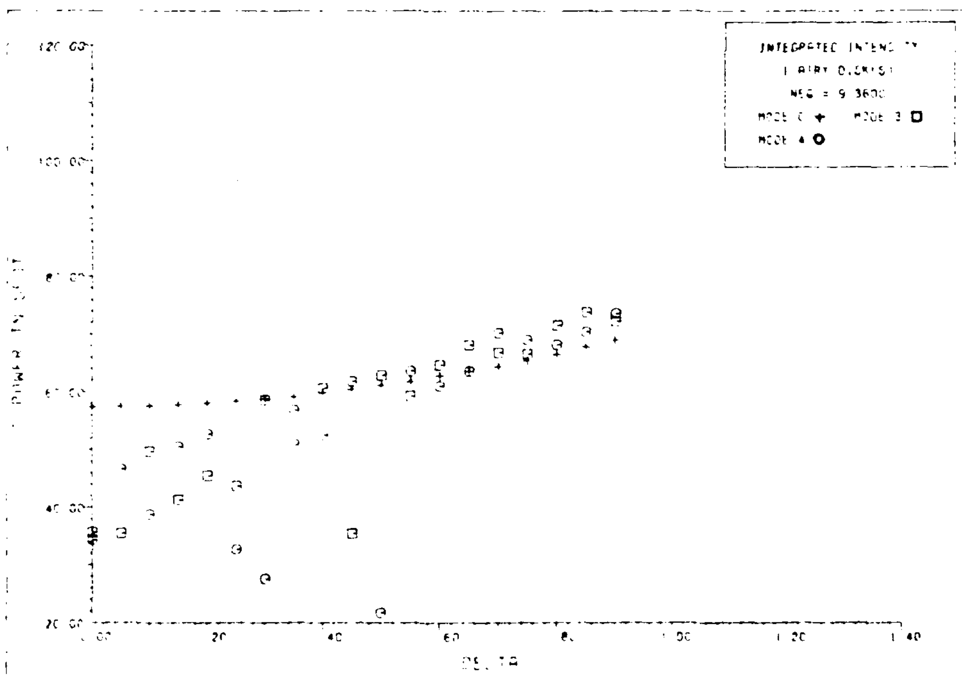

Fig. 5-9. Integrated Intensity in One Airy Disk for Modes Three and Four. $N_{eq} = 9.36$

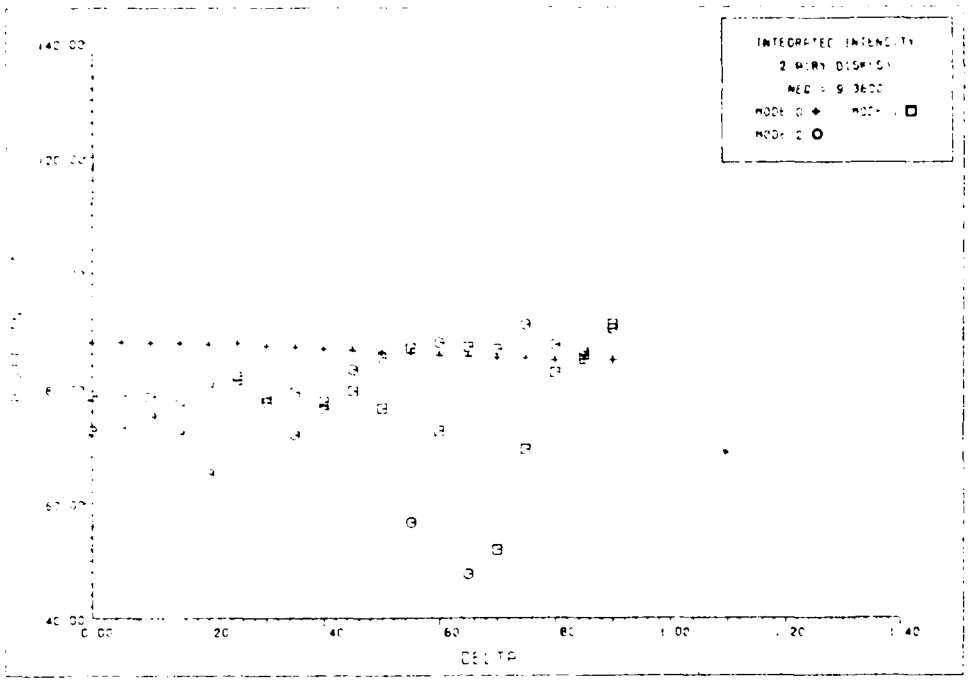

Fig. 5-10. Integrated Intensity in Two Airy Disks for Modes One and Two. $N_{eq} = 9.36$.

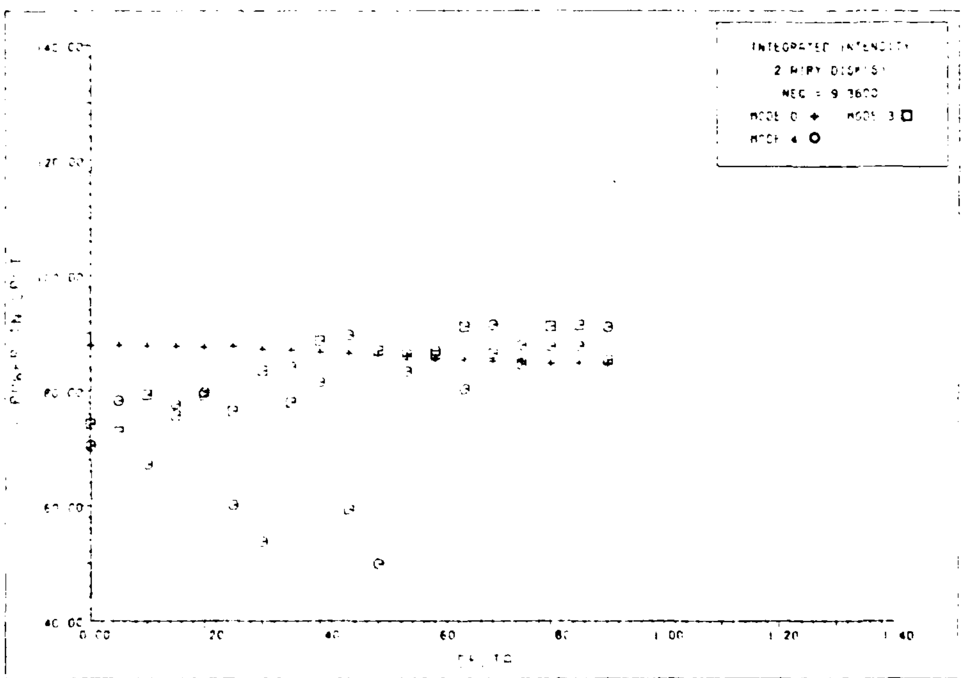

Fig. 5-11. Interated Intensity in Two Airy Disks for Modes Three and Four. $N_{eq} = 9.36$.

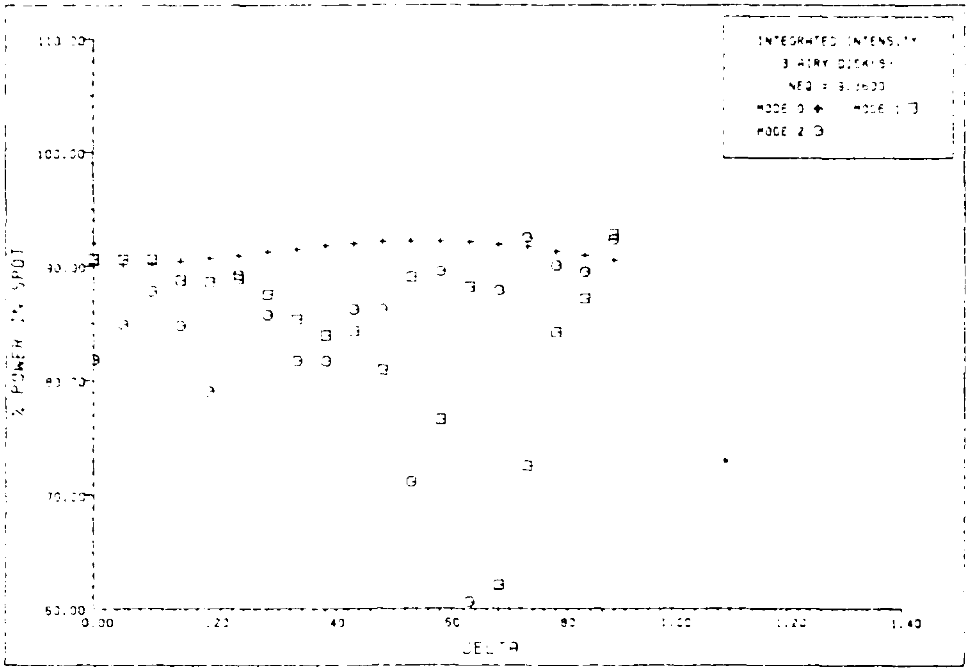

Fig. 5-12. Integrated Intensity in Three Airy Disks for Modes One and Two. $N_{eq} = 9.36$.

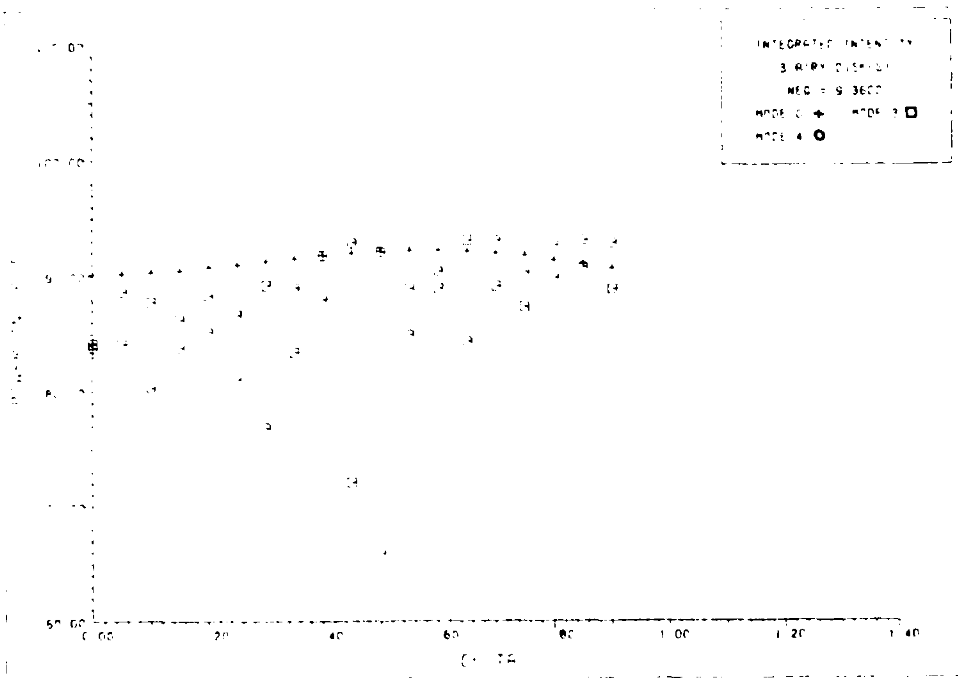

Fig. 5-13. Integrated Intensity in Three Airy Disks for Modes Three and Four. $N_{eq} = 9.36$.

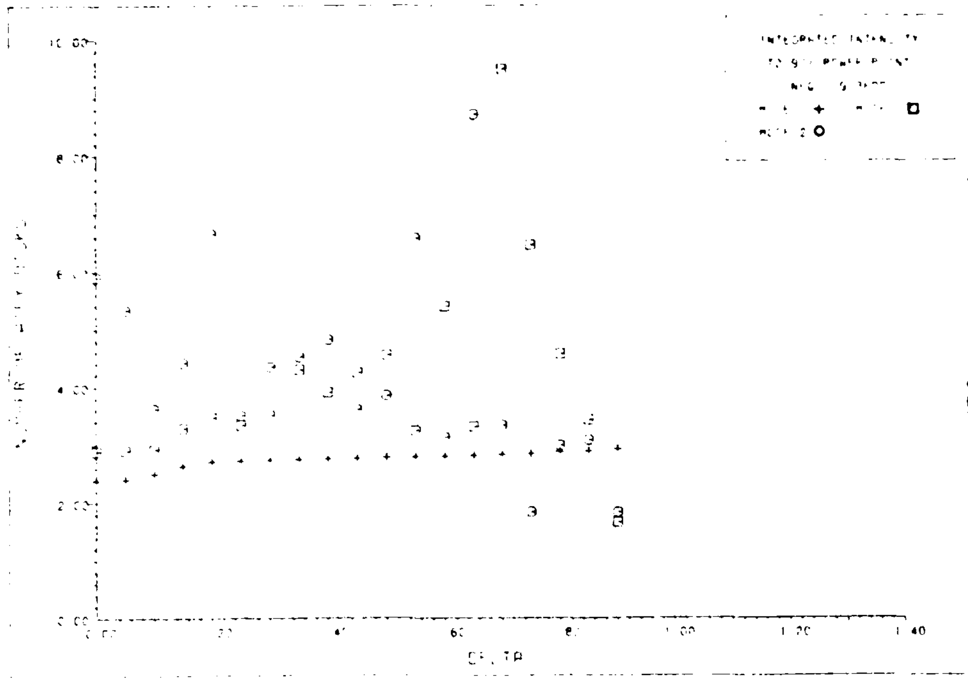

Fig. 5-14. Number of Airy Disks Required to Recover 90% of the Power for Modes One and Two. N_{eq} = 9.36.

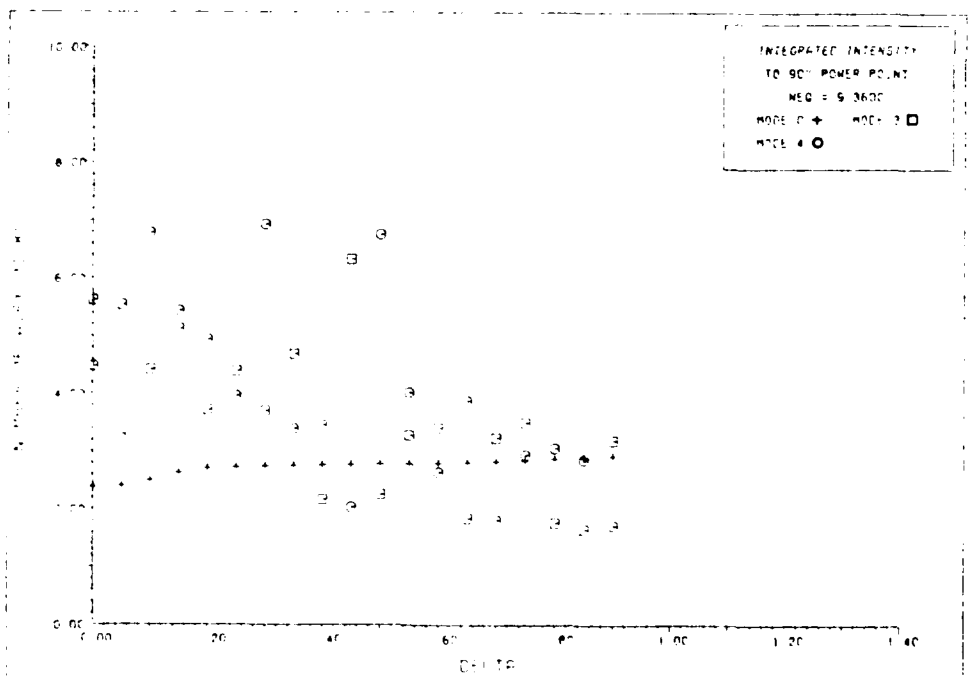

Fig. 5-15. Number of Airy Disks Required to Recover 90% of the Power for Modes Three and Four. N_{eq} = 9.36.

disks decreases slightly with increasing δ . For three Airy disks, the power first increases until $\delta = 0.6$ and then decreases. Finally, the number of Airy disks required to capture 90% of the power increases until $\delta = 0.2$ and then levels off.

For spot sizes of one and two Airy disks, all the modes show increases in integrated intensity as δ increases. The increases are more pronounced for the third and fourth modes. The increasing trend is not as obvious when the spot size is increased to three Airy disks. Modes one and two display decreasing integrated intensity for $\delta < 0.5$, and slightly increasing integrated intensity for $\delta > 0.5$. The third and fourth modes have slightly increasing integrated intensity for this spot size. The number of Airy disks required to capture 90% of the power generally decreases as δ increases. The first two modes have widely scattered values as δ increases, with only a slight downward trend. Modes three and four display less scattering and have more pronounced decreasing trends.

All modes have beam quality instabilities for $0.2 < \delta < 0.75$. At an instability, the beam quality deteriorates rapidly. Generally, the beam quality recovers from an instability within $\delta = \pm 0.05$. In some instances, a series of instabilities exists, giving the overall beam quality an oscillatory nature. The fundamental mode always exhibited an instability near $\delta = 0.7$. This instability has been noted in the literature (Ref 6:1831-2).

Individual instabilities can be traced through all three spot sizes, and affect adversely the number of Airy disks required to capture 90% of the total power. For example, the instability at $\delta = 0.7$ for the fundamental mode appears in Figures 5-8, 5-10, 5-12, and 5-14. The effect of the instability on the 90% power point is rather dramatic.

No mode appears to have better overall beam quality than the other modes. This can partially be attributed to the instabilities that all the modes suffered. In general, the fundamental mode has slightly worse beam quality than the other modes. For almost any specified δ and N_{eq} values, no method of determining a priori which mode would have the highest integrated intensity values could be developed.

All modes have comparable or better beam quality than the geometric mode for spot sizes of one and two Airy disks when $\delta > 0.6$. (This is not true at a beam quality instability.) For a spot size of three Airy disks, all modes have somewhat worse beam quality than the geometric mode, regardless of δ. All the modes require high δ values to have the same or fewer number of Airy disks to reach the 90% power point when compared to the geometric mode. Overall, at high δ values, the modes appear to have comparable or better beam quality than the geometric mode.

The percent difference $\Delta\%$ in integrated intensity for $\delta = 0.0$ and $\delta = 0.8$ is defined as

$$\Delta\% = \frac{\left(\begin{smallmatrix}\text{Power in Spot}\\ \text{with } \delta = 0.8\end{smallmatrix}\right) - \left(\begin{smallmatrix}\text{Power in Spot}\\ \text{with } \delta = 0.0\end{smallmatrix}\right)}{\left(\begin{smallmatrix}\text{Power in Spot}\\ \text{with } \delta = 0.0\end{smallmatrix}\right)} \times 100 \qquad (5.1)$$

The percent differences were calculated for all cases examined and are listed in Table III. A similar definition may be made for the percent difference in the number of spots required to capture 90% of the power:

$$\Delta'\% = \frac{\left(\begin{smallmatrix}\text{Number of Spots}\\ \text{with } \delta = 0.0\end{smallmatrix}\right) - \left(\begin{smallmatrix}\text{Number of Spots}\\ \text{with } \delta = 0.8\end{smallmatrix}\right)}{\left(\begin{smallmatrix}\text{Number of Spots}\\ \text{with } \delta = 0.0\end{smallmatrix}\right)} \times 100 \qquad (5.2)$$

The $\Delta'\%$ values are listed in Table III under the $\Delta\%$ column.

Table III reveals several interesting characteristics. In all cases, more power is deposited in one and two Airy disks when $\delta = 0.8$ than when $\delta = 0.0$. $\Delta\%$ always monotonically decreases as the spot size increases. In some instances, particularly for the fundamental mode, $\Delta\%$ is less than zero when the spot size is three Airy disks. Modes two, three, and four deposit 90% of their energy in smaller areas when $\delta = 0.8$ than when $\delta = 0.0$. These observations indicate that the power densities near the beam centroids are higher when $\delta = 0.8$ than when $\delta = 0.0$.

In general, the integrated intensity values are the highest for $\delta > 0.7$. The only major beam quality instability in this range occurs in the fundamental mode ($\delta = 0.7$). This

TABLE III

Integrated Intensity Percent Differences

Mode	N_{eq}	Case*	Δ%	Mode	N_{eq}	Case*	Δ%
1	9.36	1	60.5	3	9.36	1	100.
1	9.36	2	4.2	3	9.36	2	22.6
1	9.36	3	- 7.7	3	9.36	3	9.5
1	9.36	90	-55.2	3	9.36	90	66.9
1	9.625	1	59.9	3	9.625	1	93.2
1	9.625	2	3.6	3	9.625	2	21.6
1	9.625	3	- 7.3	3	9.625	3	7.8
1	9.625	90	-15.0	3	9.625	90	69.4
1	9.86	1	57.9	3	9.86	1	36.4
1	9.86	2	6.4	3	9.86	2	19.7
1	9.86	3	- 4.6	3	9.86	3	5.9
1	9.86	90	6.3	3	9.86	90	53.1
2	9.36	1	41.2	4	9.36	1	95.7
2	9.36	2	19.9	4	9.36	2	23.3
2	9.36	3	9.3	4	9.36	3	6.6
2	9.36	90	51.7	4	9.36	90	33.3
2	9.625	1	36.1	4	9.625	1	42.7
2	9.625	2	13.7	4	9.625	2	28.8
2	9.625	3	4.7	4	9.625	3	7.4
2	9.625	90	44.9	4	9.625	90	47.6
2	9.86	1	81.8	4	9.86	1	40.5
2	9.86	2	6.6	4	9.86	2	17.5
2	9.86	3	- 2.7	4	9.86	3	4.0
2	9.86	90	5.8	4	9.86	90	27.3

* Case refers to the number of Airy disks over which the intensity was integrated. Case of 90 refers to Δ´% values.

agrees with a conclusion from Chapter III: the beam quality should be improved at high values of δ .

Effects of Decenters on Beam Steering

The far field beam steering of the first four modes was examined for decentered resonators with N_{eq} = 9.36, 9.625, and 9.86. δ ranged from 0.0 to 0.9 in increments of 0.05. Additionally, the fundamental mode was analyzed at a much higher resolution for $N_{eq} = 9.36$. For this case, δ varied between 0.0 and 0.9 in increments of 0.01. Plots of the results for $N_{eq} = 9.36$ are presented in Figures 5-16 through 5-18.

The beam steering data were examined in three different areas. First, the data were analyzed to determine if the beam steering angles had some linear dependence on δ . Next, the oscillatory nature of the data was checked to see if a simple periodicity existed, and how the amplitude of the oscillations varied with δ . Finally, the means and standard deviations of the beam steering angles were computed and compared to one another.

The beam steering angles of the geometric mode are superimposed on Figures 5-16 through 5-18. The steering angle for any δ value is either -0.011 or -0.01 normalized half angles (nha). Since the uncertainty in the location of the centroid is approximately 0.025 nha, the optic axis lies within the error bounds. This agrees with the conclusion reached in Chapter III that the geometric mode should display no beam steering, regardless of δ .

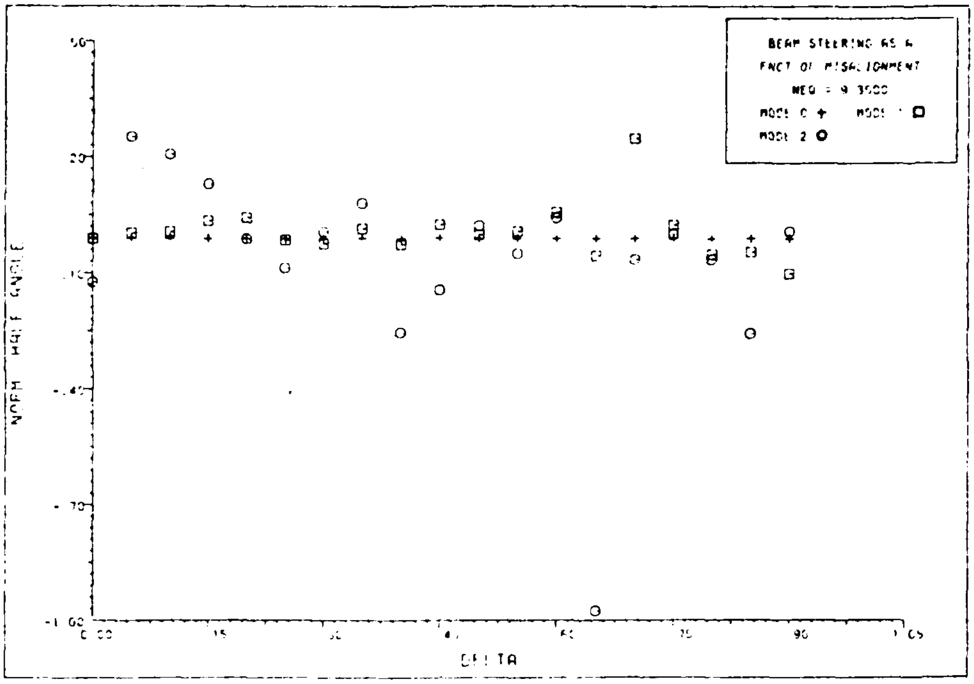

Fig. 5-16. Beam Steering Angles for Modes One and Two. N_{eq} = 9.36.

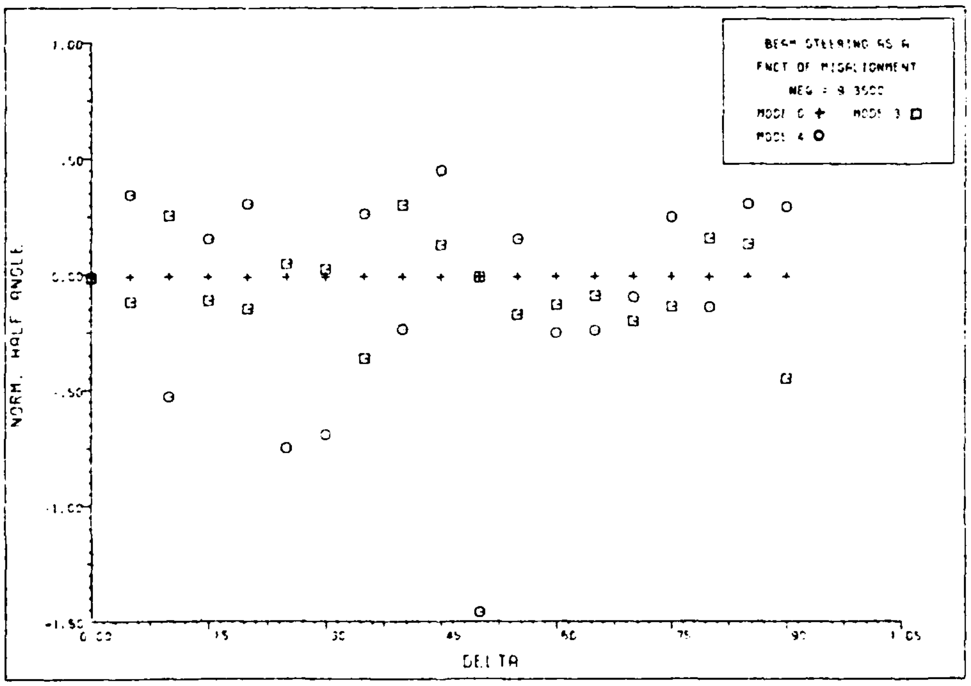

Fig. 5-17. Beam Steering Angles for Modes Three and Four. N_{eq} = 9.36.

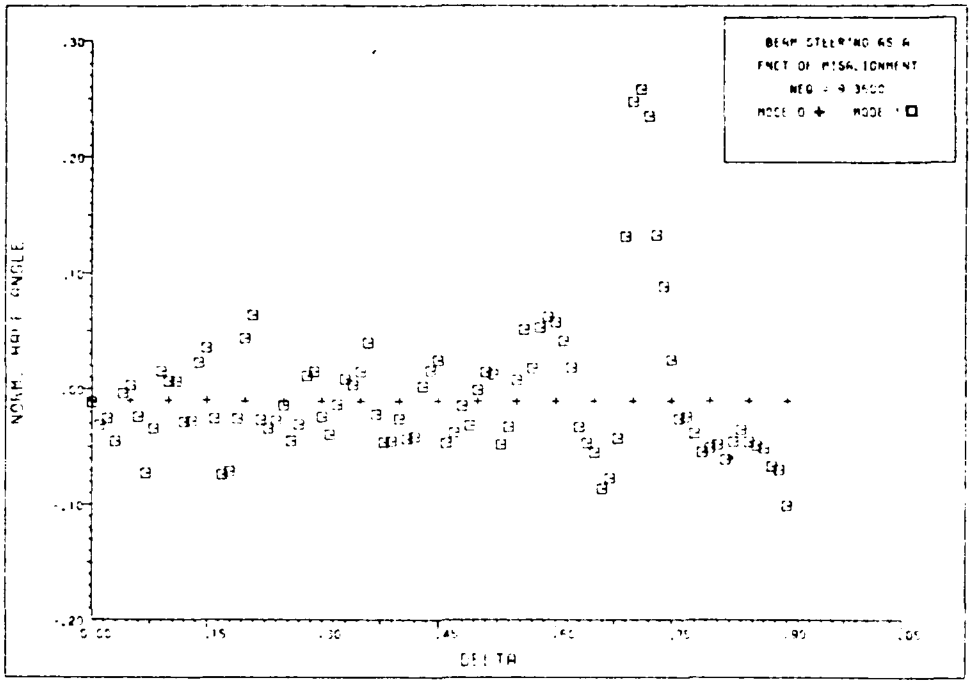

Fig. 5-18. Beam Steering Angles for Mode One Under Higher Resolution. $N_{eq} = 9.36$

No linear dependence of the beam steering angles on δ can be discerned from the plots. A linear regression was performed on the data; the results are listed in Table IV. (y_{INT}, m, and r are the y axis intercept, slope, and correlation coefficient, respectively.) The magnitudes of the correlation coefficients are less than 0.25, except in two instances. This implies that the data correlate poorly to straight line fits. Thus, the beam steering angles display no linear dependence on δ .

All the modes have beam steering angles that oscillate pseudorandomly about the optic axis. No period in δ , $N_{eq,U}$, or $N_{eq,L}$ is readily discerned. The amplitudes of

TABLE IV

Statistical Analyses Results - Beam Steering Angles

N_{eq}	Mode	y_{INT} (nha)	m (nha/unit δ)	r	$\bar{x}$ (nha)	σ (nha)
9.36	1	0.0146	-0.0186	-0.075	0.0062	0.0698
9.36	2	0.0787	-0.3244	-0.355	-0.0673	0.2565
9.36	3	0.0141	-0.1403	-0.205	-0.049	0.1924
9.36	4	-0.1935	0.2294	0.133	-0.0902	0.4865
9.625	1	-0.0017	-0.0061	-0.03	-0.0044	0.0576
9.625	2	0.0256	-0.225	-0.24	-0.0757	0.2632
9.625	3	0.0677	-0.1729	-0.271	-0.0101	0.1794
9.625	4	-0.0106	0.0943	0.095	0.0318	0.2781
9.86	1	-0.0162	0.0075	0.041	-0.0128	0.0516
9.86	2	-0.0261	-0.0507	-0.09	-0.0489	0.1583
9.86	3	-0.1311	0.0585	0.055	-0.1048	0.3016
9.86	4	-0.0181	-0.0327	-0.033	-0.0328	0.28

the oscillations appear to be random. The oscillatory nature is more apparent in the high resolution case (Figure 5-18). Again, the period does not correlate to δ , $N_{eq,U}$, or $N_{eq,L}$. It is interesting to note that the beam steering instability at $\delta = 0.71$ is coincident with a major beam quality instability (see Figure 5-8).

The mean values $\bar{x}$ and the standard deviations σ of the beam steering angles were computed for all cases. The results are listed in Table IV. The mean value is always less than 0.105 nha; in two-thirds of the cases, it is less than 0.05 nha. A rather simplistic error bound on the mean values is 0.025 nha. Thus, the mean beam steering angles are quite close to the optic axis. The standard deviations are generally less than 0.3 nha. No standard deviation exceeds 0.5 nha. The fundamental mode quite clearly has the lowest standard deviation. Its standard deviation is approximately one-third (or less) of the standard deviations of the other modes for any N_{eq} value.

In summary, the beam steering angles oscillate somewhat randomly about the optic axis. No linear dependence of the beam steering angles on δ is apparent. The average values of the beam steering angles are quite close to zero, and the standard deviations are generally less than 0.3 nha. Finally, the fundamental mode has the lowest beam steering; its standard deviation is one-third of or less than the standard deviations of the higher-order modes.

VI. Unstable Resonator Design Criteria

This chapter presents several simplified design criteria, based on the observations described in Chapter V. Design criteria for decentered resonators are presented first, followed by criteria for nondecentered resonators. It is important to realize that the comments below are based on properties of resonators with $9.3 \leq N_{eq} \leq 9.9$. The criteria may vary for resonators with N_{eq} values removed from this range.

Decentered Resonator Design Criteria

From the observations of Chapter V, highly decentered resonators offer certain advantages over nondecentered resonators. The beam quality tends to be better and the mode separation greater for highly decentered resonators. A cavity can be designed to exploit these advantages. The following guidelines are advanced for decentered resonator designs.

(1) The resonator should be designed for operation in the fundamental mode. This follows directly from the beam steering results. The fundamental mode has considerably lower beam steering angles than the higher-order modes. The standard deviations of the fundamental mode beam steering are approximately one-third or less than the standard deviations of the higher-order modes. The mean

beam steering angles for the fundamental mode are extremely close to the optic axis. Operation in the fundamental mode will generally yield the lowest beam steering angles.

(2) The resonator should be designed for very high decenters (near $\delta(K=0)$). For the particular N_{eq} range studied, δ should be approximately 0.8. This value is based on the mode separation and the separation stability, the integrated intensity, and mechanical design considerations.

The greatest separation between $|\lambda_1|$ and the magnitudes of the higher-order eigenvalues occurs for $\delta = 0.8$. This value of δ will enhance the single mode operation of the resonator. The separation is quite stable for $\delta = 0.8$; only small changes in the separation will occur if δ deviates slightly from the operating point.

Highly decentered resonators tend to deposit more energy in a given spot size than nondecentered resonators. The percent difference values recorded in Table III illustrate this point. The fundamental mode deposits more energy in spot sizes of one and two Airy disks when $\delta = 0.8$ than when $\delta = 0.0$. The overall results indicate that the power densities near the beam centroid are greater when $\delta = 0.8$ than when $\delta = 0.0$ for the fundamental mode. The higher-order modes also show beam quality improvements at high decenters. Any higher-order modes existing in the resonator would thus have

improved beam quality when $\delta = 0.8$.

The mechanical construction is simplified if the resonator is highly decentered. Nondecentered resonators typically must be built with the feedback mirror mounted on a transmissive optical element or suspended by a spyder. Consequently, the outcoupled beam is partially blocked by a mechanical element. This can be particularly bothersome if the power densities are very high. (Krupke and Sooy (Ref 17:580-1) have reported the use of an annular scraper mirror to avoid these difficulties.) In a highly decentered resonator, the spyder sizes can be reduced and the clear aperture size increased. Notably, if $\delta = 1.0$, no spyder or other interfering mechanical mounting device need block any portion of the outcoupled beam. This is illustrated in Figure 6-1.

<u>Nondecentered Resonator Design Criteria</u>

The results of the eigenvalue study suggest an optimum equivalent Fresnel number for the resonator if fundamental mode operation is desired. This value is

$$N_{eq,opt} = n + 5/8 \quad , \quad n=0,1,2,... \tag{6.1}$$

$N_{eq,opt}$ results in the best mode separation stability. Small accidental misalignments of the resonator mirrors will have little effect on the mode separation at this value of N_{eq} . Essentially, the edge waves from the feedback mirror tend to

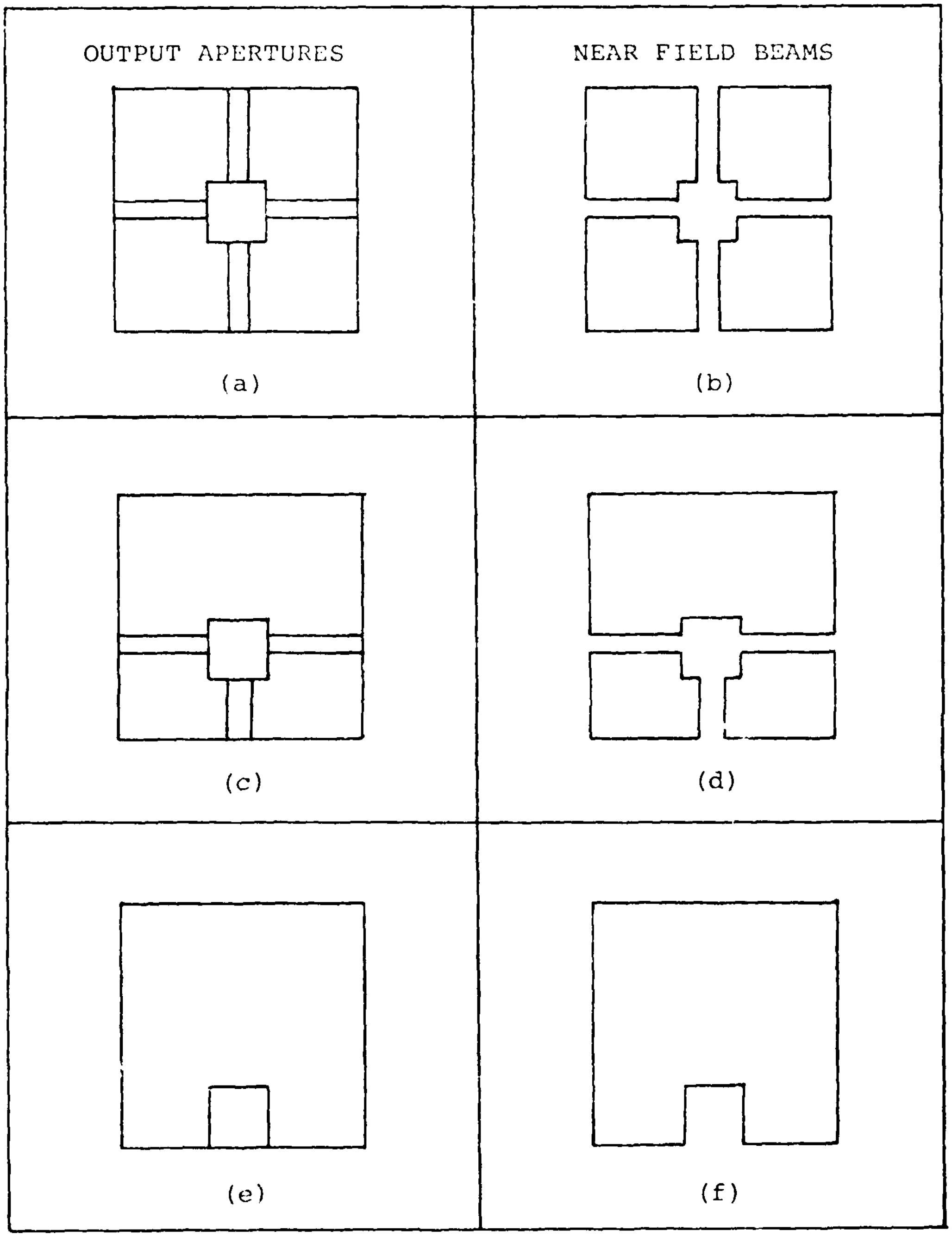

Fig. 6-1. Resonator Output Apertures and the Corresponding Near Field Beam Shapes. Note effects of the spyders and feedback mirrors on the beam shapes. (a),(b) $\delta=0$; (c),(d) $0 < \delta < 1$; (e),(f) $\delta=1$.

null each other out. The result is a relatively constant mode separation for $\delta < 0.15$. Perkins and Cason (Ref 18: 200) report a similar choice for $N_{eq,opt}$, but do not justify its choice through edge effects arguments.

Limitations

As noted in the introduction, the above design criteria are based on studies of resonators with $9.3 \leq N_{eq} \leq 9.9$. The criteria may not be particularly applicable for resonators with very high or low equivalent Fresnel numbers. Any specific design may deviate from these criteria because of effects not analyzed or considerations not taken into account in the above discussions.

VII. Conclusions and Recommendations

The conclusions of this study are summarized in this chapter. Areas that warrant additional research are outlined.

Conclusions

(1) Two equivalent Fresnel numbers, $N_{eq,U}$ and $N_{eq,L}$, can be defined for decentered resonators. $N_{eq,U}$ and $N_{eq,L}$ are functions of the feedback mirror fractional decenter δ. The defining relationships for the two Fresnel numbers are given in Eqs (2.22) and (2.23).

(2) Drawing an analogy to the case of a nondecentered resonator, two functions, $\delta(K)$ and $\delta(K')$, can be derived that yield δ values at which the separation between $|\lambda_1|$ and $|\lambda_2|$ is minimal or maximal. $|\lambda_1|$ and $|\lambda_2|$ are the magnitudes of the two lowest-order eigenvalues. K and K' are integer variables used in the functions defining $\delta(K)$ and $\delta(K')$, respectively (see Eqs (2.27) and (2.30)).

(3) The eigenvalues are functions of $N_{eq,U}$ and $N_{eq,L}$. Two types of structure are exhibited in the $|\lambda_1|$ and $|\lambda_2|$ curves: an overall structure periodic in $N_{eq,L}$, and a superimposed fine structure periodic in $N_{eq,U}$. $\delta(K)$ and $\delta(K')$ quite accurately predict the values of δ at which the separation between $|\lambda_1|$ and $|\lambda_2|$ is maximal or minimal.

(4) Major cusps in the $|\lambda_1|$ and $|\lambda_2|$ curves occur at the δ(K odd) values. The cusps undergo a regular

evolutionary pattern with four phases as N_{eq} is increased: a very deep cusp, a doubly degenerate cusp, a mode crossing with a single degenerate point, and a complete separation of the modes. The cyclic behavior is apparently related to $N_{eq,U}$, $N_{eq,L}$, and constructive and destructive edge effects from the feedback mirror.

(5) The mode separation maxima between $|\lambda_1|$ and $|\lambda_2|$ at the δ(K even) values tend to increase in magnitude as δ is increased. The greatest separation invariably occurs when $\delta \cong \delta(K=0)$. At this δ value, the mode separation is very stable.

(6) The higher-order eigenvalues interleave somewhat randomly at low δ values. The interleaving becomes regular and roughly periodic in $N_{eq,U}$ for $\delta > 0.65$. The crossings between $|\lambda_2|$ and $|\lambda_3|$ behave similarly.

(7) The power deposited in one and two Airy disks generally increases as δ increases for all modes. The trend is somewhat nebulous when the spot size is increased to three Airy disks. The number of Airy disks required to receive 90% of the power generally decreases as δ increases. This trend is somewhat vague for the fundamental mode, but is quite pronounced for the third and fourth modes.

(8) All modes display beam quality instabilities for $0.2 \leq \delta \leq 0.75$.

(9) No mode consistently deposits more energy into a given spot size than the other modes. On the average, the fundamental

mode appears to have slightly lower beam quality than the other modes.

(10) The beam steering angles have no linear dependence on δ . This is confirmed by the low correlation coefficients from the linear regression analysis.

(11) The beam steering angles for all modes fluctuate pseudorandomly about the optic axis. No periodicity in δ , $N_{eq,U}$, or $N_{eq,L}$ is readily apparent. The amplitudes of the fluctuations display no general trends with δ , $N_{eq,U}$, or $N_{eq,L}$.

(12) The means and standard deviations of the beam steering angles are lowest for the fundamental mode. The standard deviations of this mode are at least one-third as small as those of the higher-order modes. The standard deviations of all modes tend to be less than 0.3 normalized half angles, although in one case, $\delta \cong 0.5$ normalized half angles.

Recommendations

(1) The analyses of this study were performed on a limited class of resonators ($9.3 \leq N_{eq} \leq 9.9$, cavity magnification = 2). The same analyses should be performed on resonators of lower and higher equivalent Fresnel numbers and various magnifications. It should be determined if the observations and results of this study apply to other classes of unstable resonators.

(2) The beam steering angles should be correlated to the phase tilts on the output modes. The tilts might have to be weighted to account for intensity fluctuations and the asymmetric

shape of the output aperture.

(3) The beam quality instabilities might correlate to large resonator mode aberrations. This possibility should be examined, and a model developed to predict at what δ values the instabilities will occur.

(4) As noted in Chapter V, a beam quality instability and a large beam steering angle exist in the fundamental mode for $\delta = 0.71$, $N_{eq} = 9.36$. This observation should be investigated further to determine if there is a general correlation between beam quality instabilities and beam steering, or if this is merely an isolated coincidence.

Bibliography

1. Kogelnik, H. and T. Li. "Laser Beams and Resonators," Proceedings IEEE, Vol. 54, No. 10: 1312-1329 (Oct 1966).

2. Horwitz, P. "Asymptotic Theory of Unstable Resonator Modes," Journal of the Optical Society of America, 63(12): 1528-1543 (Dec 1973).

3. Berdine, Richard W. Mode Analysis in a Misaligned Unstable Resonator. MS Thesis. Wright-Patterson AFB, Ohio: School of Engineering, Air Force Institute of Technology, Dec 1981.

4. Rowley, James E. Computer Analysis of Modes in an Unstable Strip Resonator. MS Thesis. Wright-Patterson AFB, Ohio: School of Engineering, Air Force Institute of Technology, Dec 1980.

5. Horwitz, P. "Modes in Misaligned Unstable Resonators," Applied Optics, 15(1): 167-178 (Jan 1976).

6. Weiner, M.M. "Modes of Empty Off-Axis Unstable Resonators with Rectangular Mirrors," Applied Optics, 18(11): 1828-1834 (Jun 1979).

7. Fox, A.G. and T. Li. "Resonator Modes in a Maser Interferometer," Bell System Technical Journal, 40(2): 453-488 (Mar 1961).

8. Goodman, J.W. Introduction to Fourier Optics. San Francisco: McGraw-Hill, Inc., 1968.

9. Smith, M.J. "Simplified Calculation of Mode Degeneracy in Unstable Strip Resonators," Applied Optics, 20(24): 4148-4149 (Dec 1981).

10. Siegman, A.E. "Unstable Optical Resonators," Applied Optics, 13(2): 353-367 (Feb 1974).

11. Anen'ev, Y.A. and V.E. Sherstobitov. "Influence of the Edge Effects on the Properties of Unstable Resonators," Soviet Journal of Quantum Electronics, 1(3): 263-267 (Nov-Dec 1971).

12. Sutton, G.W., M.M. Weiner, and S.A. Mani. "Fraunhofer Diffraction Patterns from Uniformly Illuminated Square Output Apertures with Noncentered Square Obscurations," Applied Optics, 15(9): 2228-2232 (Sep 1976).

13. Anen'ev, Y.A., V.N. Chernov, and V.E. Sherstobitov. "Solid Laser with a High Spatial Coherence of Radiation," Soviet Journal of Quantum Electronics, 1(4):403-404 (Jan-Feb 1972).

14. Phillips, E.A., J.P. Reilley, and D.B. Northam. "Off-Axis Unstable Laser Resonator: Operation," Applied Optics, 15(9): 2159-2166 (Sep 1976).

15. Scarborough, J.B. Numerical Mathematical Analysis (5th Ed.). Baltimore: John Hopkins Press, 1962.

16. Zeimer, R.E. and W.H. Trantor. Principles of Communications - Systems, Modulation, and Noise. Boston: Houghton Mifflin Co., 1976.

17. Krupke, W.F. and W.R. Sooy. "Properties of an Unstable Confocal Resonator CO_2 Laser System," IEEE Journal of Quantum Electronics, QE-5(12): 575-586 (Dec 1969).

18. Perkins, J.F. and C. Cason. "Effects of Small Misalignments in Empty Unstable Resonators," Applied Physics Letters, 31(3): 198-200 (Aug 1977).

APPENDIX A

Far Field Intensity of the Geometric Mode

The far field intensity pattern for the geometric mode of a decentered resonator is derived in detail below. The geometric mode has a uniform amplitude and phase on any plane perpendicular to the optic axis inside the resonator (see Chapter I). The mode amplitude is exactly zero beyond the shadow boundaries. In this derivation, the amplitude is arbitrarily set equal to unity and the phase to zero.

Referring to Figure A-1, the transmission function of the output aperture of the resonator is

$$\begin{aligned} t(x) &= \mathrm{rect}\left[\frac{x - \frac{1}{2}(M+1)(1+\delta)}{(M-1)(1+\delta)}\right] \\ &+ \mathrm{rect}\left[\frac{x + \frac{1}{2}(M+1)(1-\delta)}{(M-1)(1-\delta)}\right] \end{aligned} \tag{A.1}$$

where a_2 has been normalized to unity and

$$\mathrm{rect}(x) = \begin{cases} 1 & |x| < \frac{1}{2} \\ 0 & \text{elsewhere} \end{cases} \tag{A.2}$$

Assuming that

$$z \gg \frac{kM^2}{2} \tag{A.3}$$

the Fraunhofer diffraction formula may be used. Here, z is the distance to the far field observation plane and

$k = 2\pi/\lambda'$ is the propagation constant. Then (Ref 8:61),

$$U(x_o) = \frac{\exp(ikz)\exp\left(\frac{ikx_o^2}{2z}\right)}{i\lambda' z} F[U(x)t(x)]\bigg|_{f_x = \frac{x_o}{\lambda' z}} \tag{A.4}$$

where F is the Fourier transform operator, $U(x_o)$ is the far field distribution, and $U(x)$ is the geometric mode. Performing the indicated operations yields

$$U(x_o) = \frac{\exp(ikz)\exp\left(\frac{ikx_o^2}{2z}\right)}{i\lambda' z}$$

$$\cdot \{(M-1)(1+\delta)\exp[-i\pi f_x(M+1)(1+\delta)] \operatorname{sinc}\gamma$$

$$+ (M-1)(1-\delta)\exp[i\pi f_x(M+1)(1-\delta)] \operatorname{sinc}\eta\} \tag{A.5}$$

where

$$\gamma = (M-1)(1+\delta)f_x \tag{A.6a}$$

$$\eta = (M-1)(1-\delta)f_x \tag{A.6b}$$

The far field intensity is of primary importance; it is given by the product of $U(x_o)$ and its complex conjugate $U^*(x_o)$. Denoting the intensity as $I(x_o)$, after some straightforward manipulations $I(x_o)$ reduces to

$$
\begin{aligned}
I(x_o) \quad = \quad & \frac{1}{(\lambda' z)^2}\{ (M-1)^2 (1+\delta)^2 \ \mathrm{sinc}^2\gamma \\
+ \quad & (M-1)^2 (1-\delta)^2 \ \mathrm{sinc}^2\eta \\
+ \quad & 2(M-1)^2 (1-\delta^2) \ \mathrm{sinc}\gamma \ \mathrm{sinc}\eta \ \cos[2\pi f_x (M+1)]\}
\end{aligned} \tag{A.7}
$$

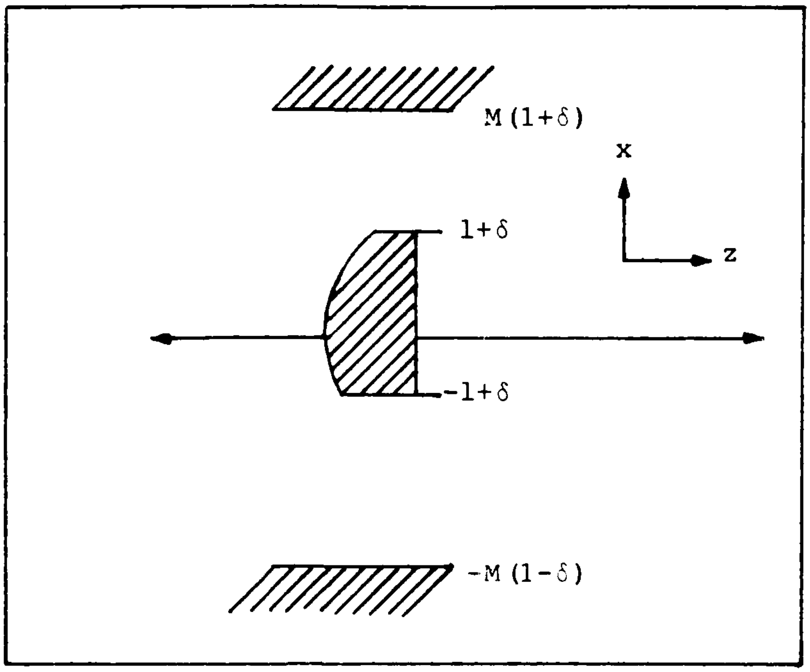

Fig. A-1. Output Aperture of the Resonator

Note a_2 has been normalized to unity.

APPENDIX B

Program Listing - EIGEN

The computer code EIGEN calculates and plots the eigenvalues of a decentered, unstable resonator. Two modes of operation are allowed: N_{eq} can be held fixed and δ varied, or δ can be held fixed and N_{eq} varied. Tables of the eigenvalues are generated and written to TAPE7. The program is essentially a modified version of the eigenvalue routine of BARC2 (Ref 3:61-74). The modifications include the provisions for iterated calculations and the addition of a plotting routine.

The required inputs are listed below. All inputs are real variables, except as noted.

IRES: flag - enter N if N_{eq} is the variable and any other letter if δ is the variable

MAG: cavity magnification

The following inputs are required if N_{eq} is the variable:

NEQMIN: minimum N_{eq} value

NEQMAX: maximum N_{eq} value

NUMNEQ: number of N_{eq} values at which the eigenvalues are to be calculated

DELMIN: δ value (fixed parameter)

The following inputs are required if δ is the variable:

DELMIN: minimum δ value

DELMAX: maximum δ value

NUMDEL: number of δ values at which the eigenvalues are to be calculated

NEQMIN: N_{eq} value (fixed parameter)

The IMSL mathematics library and DISSPLA plotting package are required for program execution. Since DISSPLA is used, the code should be submitted as a batch job.

AD-A135 854 PERFORMANCE ANALYSIS OF DECENTERED UNSTABLE RESONATORS 2/2
(U) AIR FORCE INST OF TECH WRIGHT-PATTERSON AFB OH
SCHOOL OF ENGINEERING S M RINALDI DEC 82
UNCLASSIFIED AFIT/GEO/PH/82D-12 F/G 9/1 NL

END
DATE
FILMED
1-84
DTIC

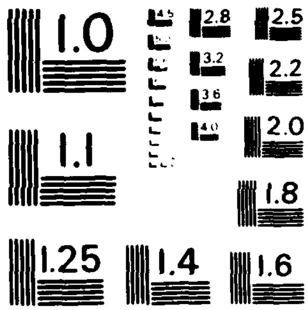

MICROCOPY RESOLUTION TEST CHART
NATIONAL BUREAU OF STANDARDS-1963-A

```
      PROGRAM EIGEN(INPUT,OUTPUT,TAPE5=INPUT,TAPE6=OUTPUT,PLFILE=5,TAPE7
     1)
C*****************************************************************
C     THIS PROGRAM CALCULATES THE EIGENVALUES OF A DECENTERED, UNSTABLE
C     STRIP RESONATOR OVER A SPECIFIED RANGE OF NEQ OR DELTA VALUES.
C     EITHER THE NEQ IS HELD FIXED AND DELTA IS VARIED, OR DELTA IS HELD
C     FIXED AND NEQ IS VARIED.  THIS PROGRAM IS ESSENTIALLY AN EXTENDED
C     VERSION OF THE EIGENVALUE ROUTINE OF BAKER (MS THESIS,
C     RICK BERDINE).
C
C     REQUIRED INPUTS:
C        IRES   = N IF NEQ IS TO BE THE VARIABLE; ANY OTHER LETTER IF
C                 DELTA IS TO BE THE VARIABLE
C        MAG    = CAVITY MAGNIFICATION
C
C        THE FOLLOWING INPUTS ARE REQUIRED IF NEQ IS THE VARIABLE:
C
C        NEQMIN = MINIMUM NEQ VALUE
C        NEQMAX = MAXIMUM NEQ VALUE
C        NUMNEQ = NUMBER OF NEQ VALUES AT WHICH THE EIGENVALUES ARE
C                 TO BE CALCULATED
C        DELMIN = DELTA VALUE (FIXED THROUGHOUT THE CALCULATION)
C
C        THE FOLLOWING INPUTS ARE REQUIRED IF DELTA IS THE VARIABLE:
C
C        DELMIN = MINIMUM DELTA VALUE
C        DELMAX = MAXIMUM DELTA VALUE
C        NUMDEL = NUMBER OF DELTA VALUES AT WHICH THE EIGENVALUES ARE
C                 TO BE CALCULATED
C        NEQMIN = NEQ VALUE (FIXED THROUGHOUT THE CALCULATION)
C
C
C     THIS PROGRAM REQUIRES THE DISSPLA GRAPHICS PACKAGE AND THE IMSL
C     MATH LIBRARY.  SINCE DISSPLA IS REQUIRED, THE PROGRAM MUST BE RUN
C     BATCH.
C
C     FINAL FORM:  22 NOVEMBER 1982.  2LT S. M. RINALDI.
C*****************************************************************
      REAL NEQ,NEQMIN,NEQMAX,MSUBN(51),MSUPN(51),NEQINC,MAG
      REAL MAG10,MAG20,MAG11,MAG21,MAG12,MAG22,MAGLAM(7)
      COMPLEX EYE,COEF(51),LAMBDA(51)
      COMPLEX LAMB11,LAMB21,LOC1
      COMPLEX CL(51),CDUM,AN1,AN2,X1,X2,Y1,Y2,Z1,Z2
      COMPLEX FALPHA(51),FBETA(51),CALPHA(51),GBETA(51)
      DIMENSION LTITLE1(2),LTITLE2(2),LTITLE3(4),XARRAY(7)
      DATA EYE,PI,INEQ/(0.,1.),3.14159265358979,1HN/
      DATA MAGLAM/7(0.)/
      READ(5,1010)IRES
 1010 FORMAT(A1)
      IF(IRES.NE.INEQ)GO TO 1020
C
C     SET UP SYSTEM FOR NEQ VARIABLE
C
      READ(5,*)NEQMIN,NEQMAX,NUMNEQ,DELMIN,MAG
      NEQINC=(NEQMAX-NEQMIN)/(NUMNEQ-1.)
      DELINC=0.
      NUMDEL=1
      GO TO 1030
C
C     SET UP SYSTEM FOR VARIABLE DELTA
C
 1020 READ(5,*)DELMIN,DELMAX,NUMDEL,NEQMIN,MAG
      DELINC=(DELMAX-DELMIN)/(NUMDEL-1.)
      NEQINC=0.
```

```
      NUMNEQ=1
      NEQMAX=NEQMIN
C
C     INITIALIZE DISSPLA PLOTTING ROUTINES
C
 1030 CALL COMPRS
      CALL BGNPL(-1)
      CALL BASALF(6HSTANDARD)
      CALL MIXALF(6HL/CGREEK)
      IF(IRES.NE.INEQ)GO TO 1040
      CALL TITLE(1H ,-1,5HNEQ,3,8HMAG((L)),8,10.,6.)
      LTITLE1(1)=10HMAG((L)) V
      LTITLE1(2)=7HS. NEQ$
      ENCODE(40,1050,LTITLE3)NEQMIN,NEQMAX
 1050 FORMAT(10HNEQ RANGE:,1X,F7.4,1X,2HTO,1X,F7.4,1H$)
      ENCODE(20,1060,LTITLE2)DELMIN
 1060 FORMAT(7HDELTA =,1X,F8.4,1H$)
      GO TO 1070
 1040 CALL TITLE(1H ,-1,5HDELTA,5,8HMAG((L)),8,10.,6.)
      LTITLE1(1)=10HMAG((L)) V
      LTITLE1(2)=9HS. DELTA$
      ENCODE(40,1080,LTITLE3)DELMIN,DELMAX
 1080 FORMAT(12HDELTA RANGE:,1X,F7.5,1X,2HTO,1X,F7.5,1H$)
      ENCODE(20,1090,LTITLE2)NEQMIN
 1090 FORMAT(5HNEQ =,1X,F8.4,1H$)
 1070 CALL HEADIN(LTITLE1,100,2,3)
      CALL HEADIN(LTITLE2,100,2,3)
      CALL HEADIN(LTITLE3,100,2,3)
      CALL MARKER(3)
      IF(IRES.EQ.INEQ)CALL GRAF(NEQMIN,5HSCALE,NEQMAX,.5,5HSCALE,1.15)
      IF(IRES.NE.INEQ)CALL GRAF(DELMIN,5HSCALE,DELMAX,.5,5HSCALE,1.15)
C
C     OUTPUT RUN DATA
C
      IF(IRES.EQ.INEQ)WRITE(7,2000)NEQMIN,NEQMAX,NEQINC,NUMNEQ,DELMIN
      IF(IRES.NE.INEQ)WRITE(7,2010)DELMIN,DELMAX,DELINC,NUMDEL,NEQMIN
 2000 FORMAT(1H1,1X,*EIGENVALUE TABLE AS A FUNCTION OF NEQ*//1X,*RANGE
     1OF NEQ: *,F8.4,1X,*TO*,1X,F8.4/1X,*NEQ INCREMENT VALUE = *,F8.6/1X
     2,*NUMBER OF NEQ VALUES = *,I3/1X,*DELTA (CONSTANT) = *,F8.6)
 2010 FORMAT(1H1,1X,*EIGENVALUE TABLES AS A FUNCTION OF DELTA*//1X,*RANG
     1E OF DELTA: *,F8.6,1X,*TO*,1X,F8.6/1X,*DELTA INCREMENT VALUE = *,F
     28.6/1X,*NUMBER OF DELTA VALUES = *,I3/1X,*NEQ (CONSTANT) = *,F8.4)
C
C     MSUPN(I) = MAG**(I-1)
C     MSUBN(I) = 1 + 1/MAG**2 + ... + 1/MAG**(2*I-2)
C
      MSUBN(1)=1.0
      MSUPN(1)=1.0
      DO 10 I=2,51
      MSUPN(I)=MAG*MSUPN(I-1)
      MSUBN(I)=MSUBN(I-1)+1./MSUPN(I)**2
 10   CONTINUE
      RNBIG=ALOG(250.*NEQMAX)/ALOG(MAG)
      IF(RNBIG.GE.50.)GO TO 777
      NBIG=INT(RNBIG)+1
      WRITE(7,996)RNBIG,NBIG
 996  FORMAT(1X,*CALCULATED NBIG = *,F8.4/1X,*SELECTED NBIG = *,I2///)
C
C     FINISH INITIALIZATIONS AND SET UP DO LOOPS
C
      NEQ=NEQMIN
      DO 2020 IINEQ=1,NUMNEQ
      T=2.*NEQ*PI*MAG*MAG/(MAG*MAG-1.)
      DELTA=DELMIN
      DO 2030 IDELTA=1,NUMDEL
C
```

```
C      COMPUTE COEFFICIENTS OF THE POLYNOMIAL
C      P(Z) = COEF(1)*Z**NDEG + COEF(2)*Z**(NDEG-1) + ...
C      + COEF(NDEG)*Z + COEF(NDEG+1)
C
       ALPHA=-1.+DELTA
       BETA=1.+DELTA
       COEF(1)=CMPLX(1.,0.)
       NDEG=2*NBIG+1
       NCOEF=NDEG+1
       M=NBIG+1
       DO 15 I=1,M
       AN1=CSQRT(4.*EYE*PI*T/MSUBN(I))
       AN2=-T*EYE/MSUBN(I)
       AN3=BETA*(1.-1./MSUBN(I+1))
       AN4=ALPHA*(1.-1./MSUBN(I+1))
       AN5=BETA-ALPHA/MSUBN(I+1)
       AN6=ALPHA-BETA/MSUBN(I+1)
       FBETA(I)=-(CEXP(AN2*AN3**2)/AN3)/AN1
       FALPHA(I)=-(CEXP(AN2*AN5**2)/AN5)/AN1
       GBETA(I)=(CEXP(AN2*AN6**2)/AN6)/AN1
       GALPHA(I)=(CEXP(AN2*AN4**2)/AN4)/AN1
15     CONTINUE
       FALPHA(M)=CEXP(AN2*BETA**2)/BETA/(-AN1)
       FBETA(M)=FALPHA(M)
       GBETA(M)=CEXP(AN2*ALPHA**2)/ALPHA/AN1
       GALPHA(M)=GBETA(M)
       COEF(2)=-(FBETA(1)+GALPHA(1)+1.)
       L1=NBIG+2
       NA=1
       NB=1
       DO 21 I=3,L1
       X2=CMPLX(0.,0.)
       Y2=X2
       DO 18 JA=1,NA
       KA=NA-JA+1
       X1=FBETA(JA)*GALPHA(KA)-FALPHA(JA)*GBETA(KA)
       X2=X1+X2
18     CONTINUE
       IF(I.EQ.3) GO TO 20
       DO 19 JB=1,NB
       KB=NB-JB+1
       Y1=FALPHA(JB)*GBETA(KB)-FBETA(JB)*GALPHA(KB)
       Y2=Y1+Y2
19     CONTINUE
       NB=NB+1
20     Z1=FBETA(I-2)-FBETA(I-1)
       Z2=GALPHA(I-2)-GALPHA(I-1)
       COEF(I)=X2+Y2+Z1+Z2
       NA=NA+1
21     CONTINUE
       L2=NBIG+3
       NA=NBIG-1
       NB=NBIG-1
       DO 28 I=L2,NCOEF
       X2=CMPLX(0.,0.)
       Y2=X2
       IF(I.EQ.NCOEF) GO TO 23
       DO 22 JA=1,NA
       KA=NBIG+JA-NA
       X1=FBETA(M-JA)*GALPHA(KA)-FALPHA(M-JA)*GBETA(KA)
       X2=X1+X2
22     CONTINUE
       IF(I.EQ.L2) GO TO 25
23     DO 24 JB=1,NB
       KB=NBIG+JB-NB
       Y1=FALPHA(M-JB)*GBETA(KB)-FBETA(M-JB)*GALPHA(KB)
```

```
      Y2=Y1+Y2
24    CONTINUE
      NB=NB-1
      GO TO 27
25    DO 26 JB=1,NBIG
      KB=NBIG-JB+1
      Y1=FALPHA(JB)*GBETA(KB)-FBETA(JB)*GALPHA(KB)
      Y2=Y1+Y2
26    CONTINUE
27    Z1=FBETA(M)*(GALPHA(I-M-1)-GBETA(I-M-1))
      Z2=GALPHA(M)*(FALPHA(I-M-1)-FBETA(I-M-1))
      COEF(I)=X2+Y2+Z1-Z2
      NA=NA-1
28    CONTINUE
C
C     COMPUTE ROOTS OF POLYNOMIAL WITH IMSL ROUTINE ZCPOLY, TO
C     OBTAIN THE EIGENVALUES, AND THEN ORDER EIGENVALUES BY
C     SIZE.
C
      CALL ZCPOLY(COEF,NDEG,LAMBDA,IER)
      WRITE(7,89)NEQ,DELTA
 89   FORMAT(1X,100(1H*)//1X,*NEQ    = *,F8.4/1X,*DELTA = *,F8.6//5X,*I*,
     12X,*LAMBDA(REAL)*,5X,*LAMBDA(IMAG)*,6X,*EVMAG*,10X,*EVPH*/)
      I=1
      DO 70 I1=2,NDEG
      SIZE= REAL(LAMBDA(I))**2+AIMAG(LAMBDA(I))**2
      K=I
      DO 75 J=I1,NDEG
      SIZE1=REAL(LAMBDA(J))**2+AIMAG(LAMBDA(J))**2
      IF(SIZE1.LT.SIZE) GO TO 75
      K=J
      SIZE=SIZE1
75    CONTINUE
      CDUM=LAMBDA(I)
      LAMBDA(I)=LAMBDA(K)
      LAMBDA(K)=CDUM
      CL(I)=LAMBDA(I)
      EVPH=ATAN2(AIMAG(CL(I)),REAL(CL(I)))*180./PI
      SMA=REAL(CL(I))**2+AIMAG(CL(I))**2
      SMAG=SQRT(SMA)
      WRITE(7,333)I,LAMBDA(I),SMAG,EVPH
 333  FORMAT(1X,I5,1X,4(G14.7,1X))
      I=I1
70    CONTINUE
      EVPH=ATAN2(AIMAG(LAMBDA(NDEG)),REAL(LAMBDA(NDEG)))*180./PI
      SMA=REAL(LAMBDA(NDEG))**2+AIMAG(LAMBDA(NDEG))**2
      SMAG=SQRT(SMA)
      WRITE(7,333)NDEG,LAMBDA(NDEG),SMAG,EVPH
C
C     SEARCH FOR MAX AND MIN MODE SEPARATIONS, AND MAX AND MIN
C     EIGENVALUES.
C
      IF(IINEQ+IDELTA-3)2040,2050,2060
 2040 MAG12=CABS(LAMBDA(1))
      MAG22=CABS(LAMBDA(2))
      SEP2=MAG12-MAG22
      GO TO 2070
 2050 LAMB11=LAMBDA(1)
      LAMB21=LAMBDA(2)
      LOC1=CMPLX(NEQ,DELTA)
      MAG11=CABS(LAMBDA(1))
      MAG21=CABS(LAMBDA(2))
      SEP1=MAG11-MAG21
      GO TO 2070
 2060 MAG1J=CABS(LAMBDA(1))
      MAG2J=CABS(LAMBDA(2))
```

```
      SEP0=MAG10-MAG20
      IF(MAG11.GT.MAG12.AND.MAG11.GT.MAG10)WRITE(7,2080)LAMB11,MAG11,LOC
     11
      IF(MAG11.LT.MAG12.AND.MAG11.LT.MAG10)WRITE(7,2090)LAMB11,MAG11,LOC
     11
      IF(MAG21.GT.MAG22.AND.MAG21.GT.MAG20)WRITE(7,2100)LAMB21,MAG21,LOC
     11
      IF(MAG21.LT.MAG22.AND.MAG21.LT.MAG20)WRITE(7,2110)LAMB21,MAG21,LOC
     11
      IF(SEP1.GT.SEP2.AND.SEP1.GT.SEP0)WRITE(7,2120)SEP1,LOC1
      IF(SEP1.LT.SEP2.AND.SEP1.LT.SEP0)WRITE(7,2130)SEP1,LOC1
      LAMB11=LAMBDA(1)
      LAMB21=LAMBDA(2)
      MAG12=MAG11
      MAG22=MAG21
      MAG11=MAG10
      MAG21=MAG20
      SEP2=SEP1
      SEP1=SEP0
      LOC1=CMPLX(NEQ,DELTA)
 2080 FORMAT(/1X,*MAXIMUM VALUE DETECTED FOR LAMBDA(1):*/3X,*LAMBDA(1) =
     1 *,F12.10,3X,F12.10/3X,*MAG(LAMBDA(1)) = *,F10.6/3X,*NEQ    = *,F8.
     24/3X,*DELTA = *,F8.6/)
 2090 FORMAT(/1X,*MINIMUM VALUE DETECTED FOR LAMBDA(1):*/3X,*LAMBDA(1) =
     1 *,F12.10,3X,F12.10/3X,*MAG(LAMBDA(1)) = *,F10.6/3X,*NEQ    = *,F8.
     24/3X,*DELTA = *,F8.6/)
 2100 FORMAT(/1X,*MAXIMUM VALUE DETECTED FOR LAMBDA(2):*/3X,*LAMBDA(2) =
     1 *,F12.10,3X,F12.10/3X,*MAG(LAMBDA(2)) = *,F10.6/3X,*NEQ    = *,F8.
     24/3X,*DELTA = *,F8.6/)
 2110 FORMAT(/1X,*MINIMUM VALUE DETECTED FOR LAMBDA(2):*/3X,*LAMBDA(2) =
     1 *,F12.10,3X,F12.10/3X,*MAG(LAMBDA(2)) = *,F10.6/3X,*NEQ    = *,F8.
     24/3X,*DELTA = *,F8.6/)
 2120 FORMAT(/1X,*MODE SEPARATION PEAK DETECTED:*/3X,*SEPARATION = *,F10
     1.6/3X,*NEQ    = *,F8.4/3X,*DELTA = *,F8.6/)
 2130 FORMAT(/1X,*MODE SEPARATION MINIMUM DETECTED:*/3X,*SEPARATION = *
     1F10.6/3X,*NEQ    = *,F8.4/3X,*DELTA = *,F8.6/)
C
C     PLOT THE FIRST SEVEN EIGENVALUES
C
 2070 NUMPLOT=7
      IF(NDEG.LT.NUMPLOT)NUMPLOT=NDEG
      DO 2140 IPLOT=1,NUMPLOT
      MAGLAM(IPLOT)=CABS(LAMBDA(IPLOT))
      IF(IRES.EQ.INEQ)XARRAY(IPLOT)=NEQ
      IF(IRES.NE.INEQ)XARRAY(IPLOT)=DELTA
 2140 CONTINUE
      CALL CURVE(XARRAY,MAGLAM,NUMPLOT,-1)
      DELTA=DELTA+DELINC
 2030 CONTINUE
      NEQ=NEQ+NEQINC
 2020 CONTINUE
      GO TO 2150
 777  WRITE(7,2160)
 2160 FORMAT(/1X,100(1H*)//1X,*PROGRAM WAS TERMINATED BECAUSE NBIG WAS O
     1UTSIDE OF ITS LIMITS.*//1X,100(1H*))
 2150 CALL ENDPL(1)
      CALL DONEPL
      STOP
      END
```

APPENDIX C

Program Listing - FOCAL

The code FOCAL performs all of the far field calculations. The resonator mode is propagated to the far field, the centroid is located, the integrated intensity is computed, and the beam steering angle is calculated. The output includes intensity profile and integrated intensity data (TAPE8) and plots (TAPE9).

The input data is read from TAPE7 and is entered interactively. The data on TAPE7 in the order required is:

MAG:	cavity magnification (real)
NEQ:	equivalent Fresnel number (real)
DELTA:	δ (real)
MODE:	mode number (integer)
ROOT:	mode eigenvalue (complex)
XMIN:	minimum x value at which the resonator mode mode is calculated (real)
XMAX:	maximum x value at which the resonator is calculated (real)
INCX:	number of points per unit x at which the mode is calculated (integer)
NDATA:	total number of points at which the mode is calculated (integer)

FIELD: the complex field values (complex)

SLOPE: slope of the phase front in the plane of the feedback mirror - required only for mode one (real)

Data entered interactively includes:

AMIN: minimum normalized half angle value at which the far field intensity is to be calculated (real)

AMAX: maximum normalized half angle value at which the far field intensity is to be calculated (real)

NUMF: total number of points at which the far field intensity is to be calculated (integer)

IRES: response to a posed question - input Y for "yes" and any other letter for "no"

CCPLOT56X or CCPLOT1038 is required to generate the Calcomp plots.

```
      PROGRAM FOCAL(INPUT,OUTPUT,TAPE5=INPUT,TAPE6=OUTPUT,TAPE7,TAPE8,TA
     1PE3)
C*********************************************************************
C
C      THIS PROGRAM TAKES THE NEAR FIELD DATA GENERATED BY
C      BARC1 (FROM TAPE7) AND PROPOGATES THE MODE TO THE
C      FAR FIELD.  A SIMPLE INTEGRATION ROUTINE DOES THE
C      FOURIER TRANSFORM FOR THE PROPOGATION.  A PLOT OF THE
C      FAR FIELD INTENSITY PATTERN IS GENERATED.  THE BEAM
C      CENTROID IS THEN LOCATED, AND THE INTEGRATED INTENSITY
C      IS CALCULATED FROM THE CENTROID.  THE INTEGRATED
C      INTENSITY IS ALSO PLOTTED.
C
C      REQUIRED INPUTS:
C
C         AMIN  =  LOWER LIMIT FOR PLOTS
C         AMAX  =  UPPER LIMIT FOR PLOTS
C         NUMF  =  TOTAL NUMBER OF POINTS AT WHICH THE FIELD
C                  IS CALCULATED
C         IRES  =  RESPONSE TO A POSED QUESTION.  ENTER Y FOR
C                  YES, AND ANY OTHER LETTER FOR NO.
C
C
C      THIS CODE REQUIRES CCPLOT1035 FOR CALCOMP PLOTS, OR
C      CCPLOT46X FOR PREVIEWING PLOTS AT A GRAPHICS
C      TERMINAL.
C
C      FINAL FORM:  7 OCTOBER 1982.  2LT S. M. RINALDI.
C
C*********************************************************************
      COMMON FIELD(600),XMIN,XMAX,XINC,DELTA,NDATA,FMIN,FMAX,FINC,NUMF,F
     1FINT(600),FLOC,FVALUE(600),FITBA(130),MAG
      COMPLEX EYE,FIELD,KOUT
      REAL MAG,NEQ
      DIMENSION LABEL(17)
      DATA LABEL/17(10H          )/
      EYE=(0.,1.)
      PI=3.14159265358979
      DATA IYES/1HY/
      READ(7,*)MAG,NEQ,DELTA,MODE,KOUT,XMIN,XMAX,INCX,NDATA
      READ(7,*)(FIELD(I),I=1,NDATA)
      IF(MODE.EQ.1)READ(7,*)SLOPE
C
C      CONDITION FIELD - SET POWER = 1. AND BLANK FIELD OVER FEEDBACK
C      MIRROR.
C
      XINC=1./INCX
      CALL CONDIT
C
C      OUTPUT RUN DATA TO CRT AND OUTPUT FILE (TAPE8)
C
      WRITE(6,10)MAG,NEQ,DELTA,XMIN,XMAX,XINC,NDATA,MODE,KOUT
      WRITE(8,10)MAG,NEQ,DELTA,XMIN,XMAX,XINC,NDATA,MODE,KOUT
   10 FORMAT(/1X,*RUN PARAMETERS (FROM DATA FILE)*//1X,*MAG    = *,F8.4/1
     1X,*NEQ    = *,F8.4/1X,*DELTA = *,F8.4/1X,*XMIN  = *,F8.4/1X,*XMAX
     2= *,F8.4/1X,*XINC  = *,F8.4/1X,*NDATA = *,I3/1X,*MODE  # *,I2/1X,*
     3MODE EIGENVALUE = *,F10.2,2X,F10.4/)
C
C      PRINT MAXIMUM ALLOWABLE SPATIAL FREQUENCY; READ DESIRED SPATIAL
C      FREQUENCY LIMITS.
C
      ALIM=INCX/4./2./MAG
      WRITE(6,30)-ALIM,ALIM
   30 FORMAT(1X,*LIMITS ON THE NORMALIZED HALF ANGLE ARE: *,F .4,* TO *,
```

```
  2 POINTS*/1X,*TO BE GENERATED:*/)
    READ(5,*)AMIN,AMAX,NUMF
    FMIN=AMIN/(2.*MAG)
    FMAX=AMAX/(2.*MAG)
    FINC=(FMAX-FMIN)/(NUMF-1.)

    CALL FFCALC

    LIST INTENSITY, IF DESIRED.

    WRITE(6,40)
40  FORMAT(/1X,*WOULD YOU LIKE A PRINTOUT AND CRT LISTING OF THE INTEN
   1SITY?*/)
    READ(5,300)IRES
300 FORMAT(A1)
    IF(IRES.NE.1YES)GO TO 50
    WRITE(6,80)
    WRITE(8,80)
80  FORMAT(/4X,*N HALF ANGLE*,7X,*INTENSITY*//)
    DO 60 I=1,NUMF
    WRITE(6,70)FVALUE(I),FFINT(I)
    WRITE(8,70)FVALUE(I),FFINT(I)
70  FORMAT(5X,F10.5,5X,E14.7)
60  CONTINUE

    PLOT INTENSITY

50  CALL PLOTS(0.,0.,9)
    LABEL(1)=10HFAR FIELD
    LABEL(2)=10HINTENSITY
    LABEL(3)=10H  DELTA =
    LABEL(13)=10H    NEQ =
    LABEL(15)=10H       MODE
    LABEL(5)=10H    MAG =
    LABEL(7)=10H  NORM. HA
    LABEL(10)=10HLF ANGLE
    LABEL(11)=10H  SCALED I
    LABEL(12)=10HNTENSITY
    ENCODE(10,90,LABEL(4))DELTA
    ENCODE(10,100,LABEL(14))NEQ
    ENCODE(10,110,LABEL(16))MODE
    ENCODE(10,120,LABEL(6))MAG
90  FORMAT(F9.5)
100 FORMAT(F8.4)
110 FORMAT(1X,*N*,1X,I2)
120 FORMAT(F4.4)
    CALL HGRAPH(FVALUE,FFINT,NUMF,LABEL,1,0,0)

    INITIALIZE FOR THE INTEGRATED INTENSITY ROUTINE

    WRITE(8,131)FLOC
131 FORMAT(/1X,*PEAK FIELD IS LOCATED AT A = *,F10.7/)
    WRITE(6,130)FLOC
130 FORMAT(/1X,*PEAK FIELD IS LOCATED AT A = *,F10.7/1X,*ENTER MINIMUM
   1 AND MAXIMUM HALF ANGLE VALUES FOR THE INTEGRATED*/1X,*INTENSITY R
   2OUTINE, AND THE NUMBER OF POINTS TO BE GENERATED:*/)
    READ(5,*)AMIN,AMAX,NUMF
    WRITE(8,132)AMIN,AMAX,NUMF
132 FORMAT(/1X,*INTEGRATED INTENSITY ROUTINE PARAMETERS:*/3X,*AMIN = *
   1,F9.5/3X,*AMAX = *,F9.4/3X,*NUMF = *,I3/)
    FMIN=AMIN/(2.*MAG)
    FMAX=AMAX/(2.*MAG)
    FINC=(FMAX-FMIN)/(NUMF-1.)
    CALL FFCALC
```

```
      CALL PITH(IDID,CENTROI)
C
C     WRITE INTEGRATED INTENSITY DATA TO TAPE5 AND OUTPUT
C
      WRITE(6,150)
 150  FORMAT(/1X,*DO YOU WANT A CRT LISTING OF THE INTEGRATED INTENSITY?
     1*/)
      READ(5,300)IRES
      IF(IRES.NE.IYES)GO TO 160
      WRITE(6,170)
 170  FORMAT(/1X,*INTEGRATED INTENSITY VALUES*/6X,*N H ANGLE*,11X,*INTEG
     1RATED*/6X,*FROM BEAM*,10X,*INTENSITY*/6X,*CENTROID*//)
      DO 180 I=1,IDID
      WRITE(6,190)FVALUE(I),PITHA(I)
 190  FORMAT(5X,F10.7,10X,F10.7)
 180  CONTINUE
 160  WRITE(5,170)
      DO 200 I=1,IDID
      WRITE(5,190)FVALUE(I),PITHA(I)
 200  CONTINUE
C
C     WRITE INTEGRATED INTENSITY DATA TO THE PLOT FILE
C
      LABEL(1)=10HINTEGRATED
      LABEL(2)=10H INTENSITY
      LABEL(11)=10HINTEGRATED
      LABEL(12)=10H INTENSITY
      CALL HGRAPH(FVALUE,PITBA,IDID,LABEL,1,0,0)
C
C     COMPUTE DIFFRACTION AND GEOMETRIC BEAM STEERING ANGLES
C
      THETA=DELTA*2.*MAG*NEQ*(MAG-1.)/(MAG+1.)
      OMEGA=2.*THETA/(MAG-1.)
      CENTROI=CENTROI*2.*MAG
      WRITE(5,210)THETA,OMEGA,CENTROI
      WRITE(6,210)THETA,OMEGA,CENTROI
 210  FORMAT(/1X,*RESONATOR AND DIFFRACTION ANGLES:*/3X,*GEOMETRIC TILT
     1ANGLE = *,E14.7/3X,*RESONATOR AXIS TILT  = *,E14.7/3X,*DIFFRACTION
     2 ANGLE       = *,E14.7)
      IF(MODE.EQ.1)WRITE(6,220)SLOPE
      IF(MODE.EQ.1)WRITE(5,220)SLOPE
 220  FORMAT(3X,*SLOPE = *,E14.7)
      CALL PLOTE(NNNNN)
      STOP
      END
C
C*****************************************************************
C
      SUBROUTINE CONDIT
C
C     THIS SUBROUTINE CONDITIONS THE FIELD OVER THE PLANE OF THE
C     FEEDBACK MIRROR.  SPECIFICALLY, FIELD VALUES ON THE MIRROR'S
C     SURFACE ARE SET TO (0.,0.).  THE INTENSITY IS THEN NORMALIZED
C     SO THAT ITS INTEGRATED VALUE IS 1.0.
C
      COMMON FIELD(600),XMIN,XMAX,XINC,DELTA,NDATA,FMIN,FMAX,FINC,NUMF,F
     1FINT(600),FLOC,FVALUE(600),PITHA(150),MAG
      COMPLEX FIELD,EYE
      REAL MAG
      PI=3.14159265358979
      EYE=(0.,1.)
      A2UPPER=1.+DELTA
      A2LOWER=-1.+DELTA
      X=XMIN
      SUM=0.
      DO 10 I=1,NDATA
```

```
      IF(X.GE.A2LOWER.AND.X.LT.ALUPPER)FIELD(I)=(0.,0.)
      FMAG=FIELD(I)*CONJG(FIELD(I))
      IP=(I/2)*2
      IF(I.EQ.1.OR.I.EQ.NDATA)GO TO 20
      IF(IP.EQ.I)SUM=SUM+4.*FMAG
      IF(IP.NE.I)SUM=SUM+2.*FMAG
      GO TO 30
 20   SUM=SUM+FMAG
 30   X=X+XINC
 10   CONTINUE
      SF=SUM*XINC/3.
      SQRSF=SQRT(SF)
      DO 40 I=1,NDATA
      FIELD(I)=FIELD(I)/SQRSF
 40   CONTINUE
      RETURN
      END
C
C*********************************************************************
C
      SUBROUTINE FFCALC
C
C     THIS SUBROUTINE PROPAGATES THE OUTPUT FIELD TO THE FAR FIELD.
C     THE PEAK INTENSITY POINT IS RETURNED ALONG WITH THE FAR FIELD
C     PATTERN.
C
      COMMON FIELD(600),XMIN,XMAX,XINC,DELTA,NDATA,FMIN,FMAX,FINC,NUMF,F
     1FINT(600),FLOC,FVALUE(600),PITHA(150),MAG
      COMPLEX FIELD,EYE,SUM,INTARG,I2PIF,SUM1
      REAL MAG
      F=FMIN
      BRIGHT=0.
      EYE=(0.,1.)
      PI=3.14159265358979
C
C     SET UP DO LOOP ABOUT F VALUES
C
      DO 10 IFO=1,NUMF
      X=XMIN
      I2PIF=-EYE*2.*PI*F
C
C     SET UP DO LOOP TO TAKE FOURIER TRANSFORM.
C     INTEGRATION TECHNIQUE - SIMPSON'S RULE.
C
      SUM=(0.,0.)
      FVALUE(IFO)=F*2.*MAG
      DO 20 IX=1,NDATA
      INTARG=FIELD(IX)*CEXP(I2PIF*X)
      IXP=(IX/2)*2
      IF(IX.EQ.1.OR.IX.EQ.NDATA)GO TO 30
      IF(IXP.EQ.IX)SUM=SUM+4.*INTARG
      IF(IXP.NE.IX)SUM=SUM+2.*INTARG
      GO TO 40
 30   SUM=SUM+INTARG
 40   X=X+XINC
 20   CONTINUE
      SUM1=SUM*XINC/3.
      FFINT(IFO)=SUM1*CONJG(SUM1)
      IF(FFINT(IFO).LT.BRIGHT)GO TO 50
      BRIGHT=FFINT(IFO)
      FLOC=F*2.*MAG
 50   F=F+FINC
 10   CONTINUE
      RETURN
      END
C
```

```
C*************************************************************************
C
      SUBROUTINE PITB(IDID,CENTROI)
C
C     THIS SUBROUTINE COMPUTES INTEGRATED INTENSITY FOR THE FAR FIELD
C     PATTERN.  BEAM CENTROID IS TAKEN AS THE POINT AT WHICH HALF THE
C     TOTAL POWER LIES ON EITHER SIDE.
C
      COMMON FIELD(600),XMIN,XMAX,XINC,DELTA,NDATA,FMIN,FMAX,FINC,NUMF,F
     1FINT(600),FLOC,FVALUE(600),PITHA(150),MAG
      COMPLEX FIELD
      REAL MAG
C
C     DETERMINE TOTAL POWER INSIDE LIMITS PREVIOUSLY ENTERED.
C
      SUM=0.
      DO 10 I=1,NUMF
      IP=I/2*2
      IF(I.EQ.1.OR.I.EQ.NUMF)GO TO 20
      IF(IP.EQ.I)SUM=SUM+FFINT(I)*4.
      IF(IP.NE.I)SUM=SUM+FFINT(I)*2.
      GO TO 10
 20   SUM=SUM+FFINT(I)
 10   CONTINUE
      POWER=SUM*FINC/3.
C
C     LOCATE BEAM CENTROID WITH AID OF A LINEAR INTERPOLATION.
C
      POWERA=POWER*1.5
      FINC2=FINC*2.
      FINC4=FINC*4.
      SUM=0.
      I=0
 40   I=I+1
      IP=(I/2)*2
      IF(I.EQ.1)GO TO 50
      IF(IP.EQ.I)SUM=SUM+FFINT(I)*FINC4
      IF(IP.NE.I)SUM=SUM+FFINT(I)*FINC2
      GO TO 60
 50   SUM=SUM+FFINT(1)*FINC
 60   IF(SUM.LT.POWERA)GO TO 40
      IF(IP.EQ.I)SUMP=SUM-FFINT(I)*FINC4
      IF(IP.NE.I)SUMP=SUM-FFINT(I)*FINC2
      CENTROI=FMIN+(I-2.)*FINC+(POWERA-SUMP)*FINC/(SUM-SUMP)
      DIST=(FMAX-FMIN)/2.
      FMAX=CENTROI+DIST
      FMIN=CENTROI-DIST
      FINC=(FMAX-FMIN)/(NUMF-1.)
      CP=CENTROI*MAG*2.
      WRITE(6,1002)CP
      WRITE(7,1002)CP
 1002 FORMAT(/1X,*BEAM CENTROID LOCATED AT A = *,E14.7)
      POWERP=POWER*100
      WRITE(6,1001)POWERP
      WRITE(7,1001)POWERP
 1001 FORMAT(/1X,*PERCENTAGE POWER IN REGION USED FOR LOCATING CENTROID
     1= *,F8.4)
      ERROR=2.*MAG*FINC
      WRITE(6,1000)ERROR
      WRITE(7,1000)ERROR
 1000 FORMAT(/1X,*MAX ERROR IN CENTROID LOCATION (IN NORM. HALF ANGLE UN
     5ITS) = *,E14.7)
      CALL FFCALC
C
C     INTEGRATE THE INTENSITY
C
```

```
      PITHA(1)=0.
      I=NUMF/2+1
      FACTOR=FINC/3.
      INDEX=I/2
      IDID=INDEX+1
      DO 70 I1=1,INDEX
      IA=2*I1-2
      IB=IA+1
      IC=IB+1
      PITBA(I1+1)=FACTOR*(FFINT(I+IA)+4.*FFINT(I+IB)+FFINT(I+IC)+FFINT(I
     1-IA)+4*FFINT(I-IB)+FFINT(I-IC))+PITHA(I1)
      FVALUE(I1)=(I1-1.)*FINC*4.*MAG
 70   CONTINUE
      FVALUE(INDEX+1)=INDEX*FINC*4.*MAG
      RETURN
      END
C
C*******************************************************************
C
      SUBROUTINE HGRAPH(X,Y,N,ID,NO,NP,NC)
      DIMENSION X(1),Y(1),ID(25) $ IF (NO.EQ.2) CALL PLOT(-1.35,2.10,-3)
      IF (NO.EQ.2) GO TO 30      $ IF (NO.LT.3) GO TO 10
      CALL SCALE(X,7.,N,1)       $ CALL SCALE(Y,5.,N,1)
 10   CALL PLOT(0.,11.,2)  $  CALL PLOT(8.5,11.,2)
      CALL PLOT(8.5,0.,2) $  CALL PLOT(0.,0.,2)
      CALL PLOT(1.35,1.35,-3)  $  CALL PLOT(0.,-.30,-2)
      IF(ID(1).EQ.999) GO TO 25
      CALL PLOT(.1,-.1,-3)       $ CALL PLOT(0.,-2.,-2)
      CALL SYMBOL(.25,.3,.07,ID(1),90.,20)
      CALL SYMBOL(.45,.3,.07, D(3),90.,20)
      CALL SYMBOL(.65,.3,.07,ID(13),90.,20)
      CALL SYMBOL(.85,.3,.07,ID(15),90.,20)
      CALL SYMBOL(1.05,.3,.07,ID(5),90.,20)
      CALL SYMBOL(1.15,.3,.07,ID(7),90.,20)
      CALL PLOT(0.,0.,3)         $ CALL PLOT(1.25,0.,2)
      CALL PLOT(1.25,2.,2)         $ CALL PLOT(0.,2.,-2)
      CALL PLOT(-.1,.1,-3)
 25   CALL PLOT(5.8,0.,-2)
      CALL PLOT(0.,-.30,-2)  $  CALL PLOT(-5.8,0.,-2)
      CALL PLOT(5.3,.75,-3)
      CALL AXIS(0.,0.,ID(9),-20,7.,90.,X(N+1),X(N+2))
      IF(NO.EQ.3) GO TO 27
      CALL AXIS(0.,0.,ID(11),20,5.,180.,Y(N+1),Y(N+2))
      GO TO 30
 27   CALL AXIS(0.,0.,ID(17),20,5.,180.,Y(N+1),Y(N+2))
 30   Y(N+2)=-Y(N+2)              $ CALL LINE(Y,X,N,1,NP,NC)
      Y(N+2)=-Y(N+2)              $ CALL PLOT(1.05,-2.10,-3)
      RETURN                      $ END
C
C*******************************************************************
C
      SUBROUTINE AXIS(XC,YC,L,NC,XL,ANG,RMIN,DR)
      DIMENSION L(1) $ A=ANG*3.14159/180. $ DX=.1*COS(A) $ DY=.1*SIN(A)
      IC=ISIGN(1,NC) $ NC=IABS(NC) $ R=.1 $ N=1 $ X=XC $ Y=YC $
 10   CALL PLOT(X,Y,3) $ X=X+DX $ Y=Y+DY $ CALL PLOT(X,Y,2)
      CALL PLOT(X-.21*DY*IC,Y+.21*DX*IC,2)
      IF(N.EQ.5) CALL PLOT(X-.42*DY*IC,Y+.42*DX*IC,2)
      IF(N.EQ.10) CALL PLOT(X-.75*DY*IC,Y+.75*DX*IC,2)
      N=MOD(N,10)+1 $ R=R+.1 $ IF(R.LT.XL) GO TO 10
      A=ANG-(IC+1)*45. $ DX=10.*DX $ DY=10.*DY
      C=-.175+.125*IC      $      D=.1-+.35*IC
      X=XC+C*DX-D*DY       $      Y=YC+C*DY+D*DX
      R=AMAX1(ABS(RMIN),ABS(RMIN+DR*XL)) $ R=ALOG10(R)
      IR=INT(ABS(R)) $ IF(R.LT.0.) IR=-(IR+1) $ IR=IR-MOD(IR,3)
      R1=RMIN/10.**IR $ DR1=DR/10.**IR  $ R=0.
 20   ENCODE(7,101,S)R1 $ CALL SYMBOL(X,Y,.07,S,A,7) $ R1=R1+DR1
```

```
      X=X+DX $ Y=Y+DY $ R=R+1. $ IF(R.LE.RL) GO TO 25
      R=(RL-.1*N*C)/2.      $      C=.1*.*IC
      X=X0+R*DX-C*DY        $      Y=Y0+R*DY+C*DX
      CALL SYMBOL(X,Y,.1,L,ANG,NC) $ IF(IP.EQ.0) RETURN
      ENCODE(5,102,S) $ CALL SYMBOL(X,Y,.07,10,S,ANG,5)
      CALL WHERE(X,Y,A)
      ENCODE(3,103,S) IR   $ CALL SYMBOL(X,Y,.07,S,ANG,3)
101   FORMAT(F7.2)
102   FORMAT(5H  *10)
103   FORMAT(I3)
      RETURN      $      END
C
C           SUBROUTINE SCALE(DATA,LENGTH,N,K)
C
C        REAL DATA = N+2 DIMENSIONED ARRAY OF DATA TO BE SCALED
C        INTEGER N = NUMBER OF DATA POINTS
C        REAL LENGTH = LENGTH OF THE PLOT AXIS (E.G. IN INCHES)
C        INTEGER K = UNUSED PARAMETER INCLUDED FOR COMPATIBILITY
C                    WITH THE EQUIVALENT CALCOMP SUBROUTINE
C
C        THE FOLLOWING VALUES ARE RETURNED:
C
C                DATA(N+1) = ADJUSTED DATA MINIMUM
C                DATA(N+2) = "NICE" SCALE FACTOR IN DATA UNITS
C                            PER LENGTH UNIT (E.G. VOLTS/INCH)
C
C***************************************************************
C
      SUBROUTINE SCALE(DATA,LENGTH,N,K)
      REAL DATA(1), LENGTH, SF(5)
      DATA SF /1., 2., 2.5, 5., 10. /

C     COMPUTE THE RAW SCALE FACTOR

      DMIN=DMAX=DATA(1)
      DO 10 I=1,N
            IF(DATA(I) .LT. DMIN) DMIN = DATA(I)
            IF (DATA(I). GT. DMAX) DMAX = DATA(I)
10    CONTINUE
C
C     EXCLUDE TRIVIAL ERROR CASES
C
      DATA(N+1) = DMIN
      DATA(N+2) = 1.0
      IF (LENGTH .LE. 0.0 .OR. DMAX .EQ. DMIN )  RETURN
      RAWSF = (DMAX - DMIN) / LENGTH

C     RAWSF = SFMANT * 10. ** SFEXP, WHERE 1 .LE. SFMANT .LT. 10

      SFEXP = AINT( ALOG10( RAWSF ) )
      IF ( RAWSF .LT. 1.0 ) SFEXP = SFEXP - 1.0
      SFMANT = RAWSF * 10.0 ** (-SFEXP)

C     LOCATE NEXT LARGER "NICE" SCALE FACTOR

      DO 20 I=1,5
20    IF ( SF(I) .GT. SFMANT )  GO TO 30
      PRINT*," SCALE: SCALE FACTOR ERROR ... "  $  RETURN
30    SFNICE = SF(I) * 10.  ** SFEXP

C     COMPUTE ADJUSTED DATA MINIMUM

      ADJMIN = AINT ( DMIN / SFNICE ) * SFNICE
      IF ( ADJMIN .GT. DMIN ) ADJMIN = ADJMIN - SFNICE
      IF ( (DMAX - ADJMIN) / SFNICE .LE. LENGTH )  GO TO 40
```

```
C     NEED TO USE THE NEXT LARGER SCALE FACTOR

      IF ( I .LT. 5 )  SFNICE = SF(I+1) * 10.0 ** SFEXP
      IF ( I .EQ. 5 )  SFNICE = 20.0     * 10.0 ** SFEXP
      ADJMIN = AINT ( DMIN /  SFNICE ) * SFNICE
      IF ( ADJMIN .GT. DMIN) ADJMIN = ADJMIN - SFNICE
40    CONTINUE
      DATA(N+1) = ADJMIN
      DATA(N+2) = SFNICE
      RETURN
      END
```

Vita

Steven M. Rinaldi was born on 28 November 1958 in Passaic, New Jersey. He graduated from Jenks High School, Jenks, Oklahoma, in May 1976. He attended the University of Oklahoma from August 1976 to May 1981. He graduated with a B.S. degree in Electrical Engineering and was commissioned on 20 December 1980. His initial active duty assignment was to the Air Force Institute of Technology, Wright-Patterson Air Force Base, Ohio.

Permanent Address: 8435 S. Quebec
Tulsa OK 74136

UNCLASSIFIED
SECURITY CLASSIFICATION OF THIS PAGE (When Data Entered)

REPORT DOCUMENTATION PAGE		READ INSTRUCTIONS BEFORE COMPLETING FORM
1. REPORT NUMBER AFIT/GEO/PH/82D-12	2. GOVT ACCESSION NO.	3. RECIPIENT'S CATALOG NUMBER
4. TITLE (and Subtitle) PERFORMANCE ANALYSIS OF DECENTERED UNSTABLE RESONATORS		5. TYPE OF REPORT & PERIOD COVERED MS Thesis 6. PERFORMING ORG. REPORT NUMBER
7. AUTHOR(s) Steven M. Rinaldi 2Lt USAF		8. CONTRACT OR GRANT NUMBER(s)
9. PERFORMING ORGANIZATION NAME AND ADDRESS Air Force Institute of Technology (AFIT/EN) Wright-Patterson AFB, Ohio 45433		10. PROGRAM ELEMENT, PROJECT, TASK AREA & WORK UNIT NUMBERS
11. CONTROLLING OFFICE NAME AND ADDRESS Air Force Institute of Technology (AFIT/EN) Physics Dept. Wright-Patterson AFB, Ohio 45433		12. REPORT DATE 17 December 1982 13. NUMBER OF PAGES 102
14. MONITORING AGENCY NAME & ADDRESS(if different from Controlling Office) Air Force Institute of Technology (AFIT/EN) Physics Dept. Wright-Patterson AFB, Ohio 45433		15. SECURITY CLASS. (of this report) UNCLASSIFIED 15a. DECLASSIFICATION/DOWNGRADING SCHEDULE

16. DISTRIBUTION STATEMENT (of this Report)

Approved for public release; distribution unlimited.

17. DISTRIBUTION STATEMENT (of the abstract entered in Block 20, if different from Report)

18. SUPPLEMENTARY NOTES

Approved for public release: IAW AFR 190-17.
LYNN E. WOLAVER
Dean for Research and Professional Development
Air Force Institute of Technology (ATC)
Wright-Patterson AFB OH 45433
12 SEP 1983

19. KEY WORDS (Continue on reverse side if necessary and identify by block number)

Misaligned Resonator
Unstable Resonator
Off-Axis Resonator
Decentered Resonator
Mode Eigenvalue
Integrated Intensity
Beam Steering

20. ABSTRACT (Continue on reverse side if necessary and identify by block number)

The mode eigenvalues, far field integrated intensity, and far field beam steering angles of unstable, decentered strip resonators were studied. The resonators examined had magnifications of 2.0 and equivalent Fresnel numbers in the range $9.3 \leq N_{eq} \leq 9.9$. The resonator modes were calculated by the asymptotic method of Horwitz.

Two equivalent Fresnel numbers for the decentered resonators were

DD FORM 1 JAN 73 1473 EDITION OF 1 NOV 65 IS OBSOLETE

UNCLASSIFIED
SECURITY CLASSIFICATION OF THIS PAGE (When Data Entered)

defined. The fundamental and second-order mode eigenvalues exhibited periodicities in the equivalent Fresnel numbers. The mode separation was observed to be a function of the amount of decenter and the two equivalent Fresnel numbers. The cusps of the first two eigenvalues were cyclic in N_{eq}.

The far field integrated intensity was computed for spot sizes of one, two, and three Airy disks. The percentage of total power deposited in a given spot size increased as the decenter increased. Beam quality instabilities were observed in all modes.

The beam steering angles of the first four modes were calculated. The angles fluctuated about the optic axis as the decenter was increased. The fundamental mode had significantly lower beam steering than the higher-order modes.